Review

Recent Progress in Multifunctional Gas Sensors Based on 2D Materials

Zhifang Liu [1,†], Zirui Qiao [2,†], Chen-Yuan Li [3] and Yilin Sun [1,*]

1   School of Integrated Circuits and Electronics, Beijing Institute of Technology, Beijing 100081, China; lzf@bit.edu.cn
2   Department of Chemistry, Tsinghua University, Beijing 100084, China; qzr20@mails.tsinghua.edu.cn
3   Key Laboratory of Advanced Light Conversion Materials and Biophotonics, Department of Chemistry, Renmin University of China, Beijing 100872, China; lichenyuan@ruc.edu.cn
*   Correspondence: sunyl@bit.edu.cn
†   These authors contributed equally to this work.

Abstract: The detection of specific gas components under various working conditions while at the same time realizing other functions with the same devices has emerged through great efforts due to these devices' superior energy-saving and high-efficiency properties. Although so-called multifunctional gas sensors have been fabricated with various novel materials, two-dimensional (2D) materials with unique physical and chemical properties used in multifunctional gas sensors have not yet been well studied. In this review, we summarize up-to-date multifunctional gas sensors based on different 2D materials, including graphene and its derivatives, transition metal dichalcogenides (TMDs), MXenes, etc. The progress of machine learning and artificial intelligence used in emerging powerful sensors is introduced. Their sensing abilities and mechanisms are discussed, and further smart devices equipped with IoT platforms and 5G communication are expected for future electronic use.

Keywords: gas sensors; multifunction; graphene; TMDs; MXenes

1. Introduction

With the increasing global awareness of environmental monitoring, workplace safety supervision, healthcare, and counter-terrorism efforts, gas sensors have garnered significant attention across various domains. Their pivotal role in effectively detecting hazardous gases (CO_2, CO, NO_2, etc.), targeted disease gases (NH_3, H_2S, etc.), humidity, and explosives (volatile organic compounds) has made them indispensable tools in addressing these crucial challenges [1–3]. From indoor air quality to harmful gas emissions in industrial production processes, the ability to accurately and efficiently measure gases plays a vital role in safeguarding our well-being. Moreover, it is crucial to successfully distinguish multiple gases, for example, H_2 in air and other gases, which could form potentially explosive mixtures. Electrochemical sensors have been applied to solve the issue, implying potential fire-control applications [4,5]. Numerous clinical studies have also established associations between specific constituents of volatile molecules found in exhaled human breath and a range of significant ailments, including COVID-19, asthma, diabetes, acute respiratory distress syndrome, renal and liver diseases, lung cancer, and numerous other medical ailments [3]. Up to now, the development of intelligent microsystems has been hindered by the limitations of single-function materials, which entail complex integration manufacturing processes and unsatisfactory electrochemical/sensing performance [6]. Moreover, a cross effect arises from the assessment of unwanted substances, which distorts the accuracy of measurements [4].

The versatility of flexible, stretchable, and wearable gas sensors has captured significant interest due to their wide-ranging applications, from electronic skins to health-monitoring systems [7,8]. Of particular note is their integration with strain sensors, offering

a multifunctional capability for detecting both human motions and gases over the full range [9], which holds great promise for preventive medicine and healthcare. As the future of gas sensor development unfolds, it becomes imperative to explore novel device design concepts to further enhance their potential and impact [10–12].

In the entire gas sensor fabrication process, the most crucial stage is undeniably the selection of the core sensing material. Among most of the promising sensing candidates, 2D material-based chemical gas sensors receive the most attention, because they possess an intrinsic large surface area and various absorption sites for the specific sensitive detection of different molecules, including graphene and its derivates [13,14], MXenes [15], transition metal dichalcogenides (TMDs) [16], black phosphorous [17], etc. The exceptional suitability of 2D materials for room- or low-temperature gas sensing can be attributed to their high surface accessibility, distinctive structural characteristics, and remarkable physicochemical properties [18]. The distinctive 2D geometry of these materials offers a direct exposure of the active sites to analyte molecules, creating a short mass transport pathway that facilitates rapid response and recovery times [19]. Aside from their promising sensing ability, 2D materials also possess properties like high mechanical strength, high conductivity, tunable electronic structure, etc., which make them candidates for multifunctional gas sensors (Figure 1). Here in this review, multifunctional gas sensors based on different 2D materials are summarized and discussed, especially those focused on graphene, TMDs, and MXenes. Moreover, different kinds of applications are illustrated, including motion detection, photodetection, temperature sensing, pressure sensing, and human healthcare. Smart gas sensors for artificial intelligence are also illustrated. We aim to give a new perspective for the future development of sensors and encourage practical applications of research in this area.
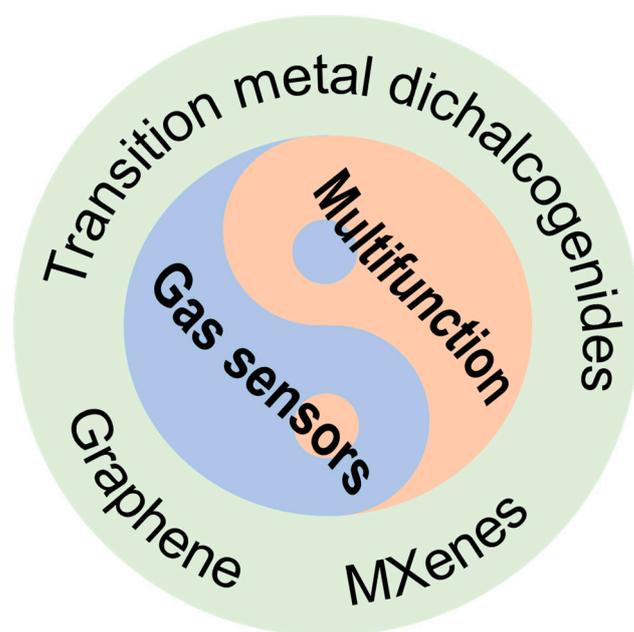

Figure 1. Schematic illustration of 2D material-based multifunctional gas sensors.

2. Multifunctional Gas Sensors Based on Different 2D Materials

In this section, graphene, TMDs, MXenes, 2D MOFs, and g-C$_3$N$_4$ are selected as representative 2D materials, whose properties range widely and almost cover all kinds of multifunctional gas-sensing devices. For each material, their unique characteristics are discussed and compared, and the pioneering works are summarized.

2.1. Graphene and Its Derivatives

Carbon-based materials have garnered significant attention due to their exceptional attributes, including superior electrical conductivity, flexibility, thermal stability, and low toxicity [20], showing applications in biomedical engineering, catalysis, flexible electronics, and sensors [21]. Among them, graphene and its derivatives, including graphene oxide (GO), reduced graphene oxide (rGO), and heteroatom-doped graphene, etc., stand out for their natural 2D properties. Graphene-based gas sensors inherit several advantages, including a high specific surface area for adsorbing and sensing gas molecules, outstanding electrical conductivity, and excellent mechanical properties, which facilitate the facile processing of various electronic devices [22]. Furthermore, the majority of graphene-based gas sensors offer the advantage of operating at room temperature, which proves highly advantageous for practical gas-sensing applications, as it ensures both applicability and energy efficiency. It is well known that perfect graphene has a zero bandgap with Dirac cone and semimetal properties [23], which is unsatisfying for sensors. Physical and chemical modifications, including architectural design, defect engineering, surface functionalization, elemental doping, etc., have been introduced to enhance the sensing ability of graphene. Therefore, most modified graphene-based materials reveal p-type semiconductor behavior, showing a tendency to adsorb O_2 and H_2O molecules in air [22]. In the case of oxidizing gases such as NO_2, SO_2, and Cl_2, which possess electron-withdrawing abilities, the concentration of the primary charge carriers (holes) on graphene increases due to the decrease in electron concentration. Consequently, the conductivity of the graphene-based sensor improves, manifesting the sensing signal as a reduction in resistance. Conversely, when it comes to reducing gases like NH_3, CO, and H_2S, which have electron-donating abilities, the sensor demonstrates a sensing signal characterized by an increase in resistance [24].

Attributed to the unique physical and chemical properties of graphene and its derivates, multifunctional graphene-based gas sensors integrating various applications have been widely reported (Table 1) [6,25–33]. Intrinsic graphene possesses remarkably high electrical conductivity and mechanical strength and a substantial specific surface area, rendering it an outstanding platform for chemical sensing applications [24,34–36]. Nevertheless, the prevalent gas nanosensors predominantly rely on electrical methods or refractive index sensing, which typically lack the ability to identify specific molecular species. Addressing this limitation, Dai et al. [37] made a significant breakthrough with the label-free identification of gas molecules through the detection of their rotational–vibrational modes using graphene plasmon. Graphene nanoribbons with 25–100 nm widths were filled up to 90% for broad midinfrared spectral range plasmon-field enhancement. The fabricated sensing device was equipped with a high-precision piezometer, a flowmeter, and a home-made infrared-transparent gas chamber (Figure 2A, left). The graphene plasmon devices for the specific recognition of NO, N_2O, NO_2, and SO_2 were tested in real time and under low concentrations (800 ppm for SO_2). Aside from real-time analysis, the components of the gas could also be monitored during chemical reactions (NO oxidation reaction) (Figure 2A, right). The chamber filled with reactant NO gas was clearly identified at 1838 and 1906 cm^{-1} based on its rotational–vibrational mode, whose intensity decreased with the injection of O_2 and the emergence of new peaks at 1590 and 1610 cm^{-1}, which coincided with the rotational–vibrational mode of NO_2. These real-time measurements exhibit exceptional selectivity, enabling direct observation of chemical reactions—a capability with tremendous potential for applications that demand in situ analysis of chemical processes [37].

Table 1. Summary of multifunctional gas sensors based on graphene and its derivatives.

Sensing Materials	Target Gas	Functions	Ref.
Au@rGO/GaN	CO	• Photodetectors for UV detection	[25]
Graphene quartz fiber	Acetone, ethanol, etc.	• Electrothermal properties	[26]
GO	Humidity	• Temperature sensor • Flow sensor	[27]
GN/PA66	Formic acid, DMF, etc.	• Human motion detection • Temperature sensing	[28]
Laser-induced graphene	NO_x	• Sensing of environment and breath analysis	[29]
rGO/WO$_3$	H_2S	• Photodegradation of dye	[30]
GO/silk fibroin	Humidity	• Health management	[31]
mPANI/G	NH_3	• Zinc ion microbattery • Dendrite-free zinc anode	[6]
MoS$_2$/graphene	NH_3	• Supercapacitors	[32]
Cu$_x$O-PPy@GO	H_2S	• Visual detection with smartphone	[33]

As mentioned before, graphene itself possesses a zero bandgap that hinders its sensing ability, which could be overcome by modification and hybridization. A notable technique, laser-induced graphene (LIG), offers a simple and rapid synthesis of porous graphene, providing numerous active surface sites for gas–solid interactions, thus significantly boosting gas-sensing capabilities [38]. With the modified laser processing parameters (0.6 W, 500 PPI image density, and 0 mm focus), the obtained LIG electrode with needle morphology exhibited impressive performance characteristics, including the largest response of 4‰, rapid response and recovery times of 113/296 s, and an ultrahigh signal-to-noise ratio (SNR) of 463 to 1 ppm NO at room temperature. The sensitivity to NO_x against other gas molecules was attributed to the lower LUMO of NO_x molecules, making LIG a potential candidate to distinguish trace NO_X from dominant CO_2 and other interfering reducing gases. The high sensitivity of LIG to NOx over other gas molecules could be attributed to the lower LUMO of NOx molecules, making LIG capable of distinguishing low-concentration NO_x from high-concentration CO_2 and other interfering gases with reducing characteristics (Figure 2B) [29]. Taking advantage of the excellent specific sensing ability of LIG and the water-resistant property of the PDMS membrane, breath analysis of patients with asthma/chronic obstructive pulmonary disease (COPD) could be conducted with NO_X biomarkers [29].
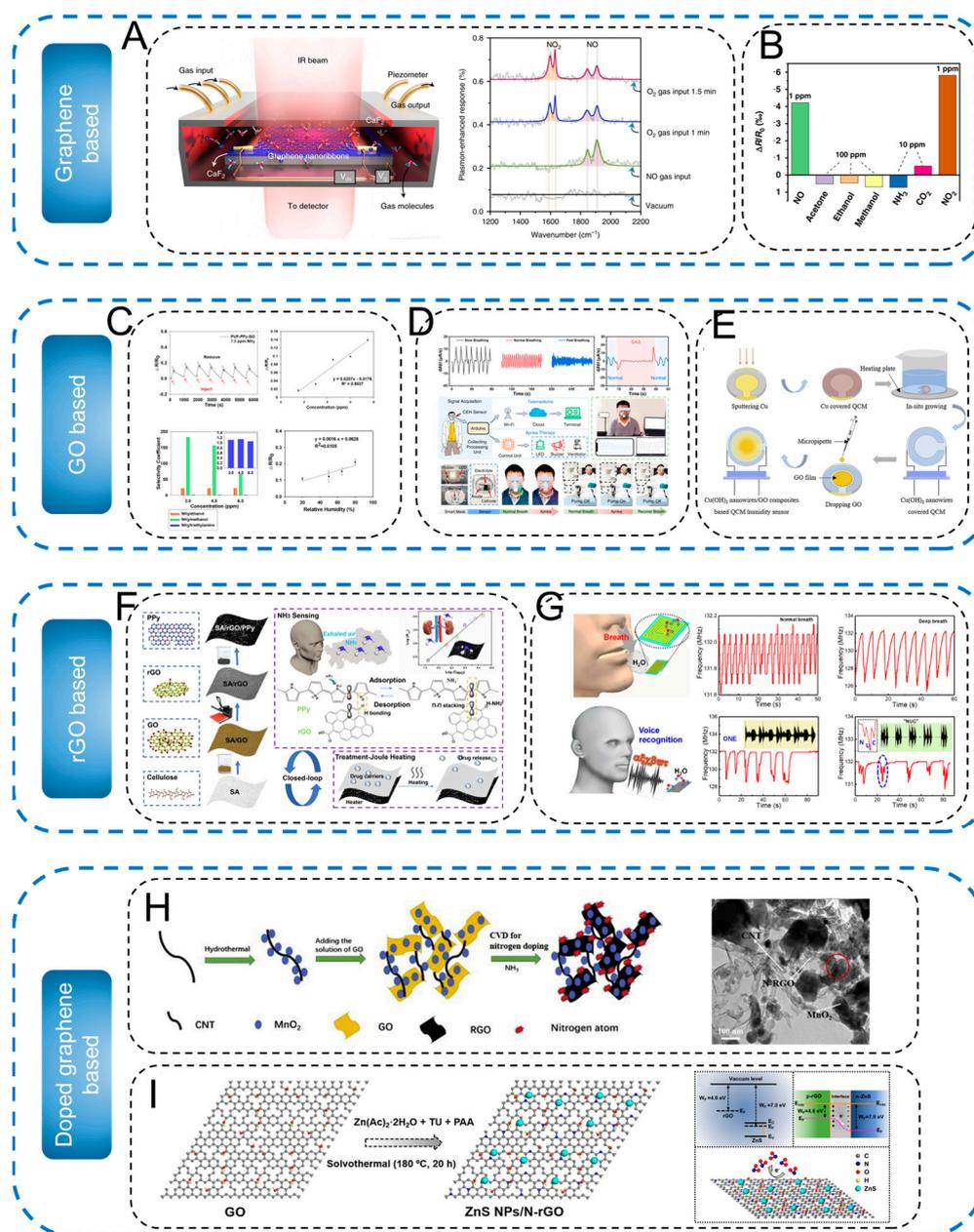
Figure 2. (**A**) **Left**: Experimental scheme of graphene-based plasmon device for gas identification. **Right**: Identification of gas molecules during chemical reactions. (Reproduced with permission from [37]. Copyright 2019, Springer Nature). (**B**) Selectivity test of the gas sensor based on laser-induced graphene to NO_x over other interfering gases. (Reproduced with permission from [29]. Copyright 2022, Springer Nature). (**C**) Gas-sensing performance of PUF-PPy-GO. (Reproduced with permission from [39]. Copyright 2021, Elsevier). (**D**) Applications of the self-powered chemoelectric humidity (CEH) sensors in respiratory monitoring, telemedicine, sleep apnea syndrome (SAS) diagnosis, and treatment. (Reproduced with permission from [31]. Copyright 2021, Springer Nature). (**E**) Schematic illustration of $Cu(OH)_2$ nanowire/GO composite-based QCM humidity sensor. (Reproduced with permission from [40]. Copyright 2020, Elsevier). (**F**) Schematic of the fabrication of SA/rGO/PPy composite fabric and corresponding NH_3 sensor and wearable closed-loop point-of-care. (Reproduced with permission from [41]. Copyright 2021, Elsevier). (**G**) Schematic setup for the sensor to monitor human breath and speech from the mouth with corresponding sensor frequency spectra. (Reproduced with permission from [42]. Copyright 2021, Elsevier). (**H**) **Left**, process for the

construction of the 3D N-rGO/CNT-MnO$_2$ hybrid. **Right**, TEM images of as-prepared N-rGO/CNT-MnO$_2$ composites. (Reproduced with permission from [43]. Copyright 2020, Elsevier). (**I**) **Left**, schematic of the synthetic process of ZnS NPs/N-rGO. **Right**, energy band diagram of rGO-ZnS and corresponding proposed sensing mechanism. (Reproduced with permission from [44]. Copyright 2021, Elsevier).

Graphene oxide (GO) and reduced graphene oxide (rGO) are the most widely studied derivatives of graphene. GO is obtained by the strong oxidation of graphene under acidic conditions (Hummer's methods) with modified surface oxygen-containing groups such as carboxyls, epoxides, and hydroxyls, which are beneficial for the adsorption of gas molecules [45]. However, the introduction of functional groups to GO inevitably causes topological defects in the graphene lattice at the same time, which leads to a decrease in electrical conductivity. Therefore, a controlled reduction (chemical, thermal, UV, etc.) of GO for the production of rGO could reobtain electrical conductivity, as well as showing more defects and dangling bonds than pristine graphene, resulting in better sensing properties [46]. Combined with other materials forming heterostructures, GO and rGO with different properties enable sensing applications in different working environments. For example, polyurethane foam (PUF)–polypyrrole (PPy) integrated with GO was synthesized via impregnation, making the surface morphology smoother due to the uniform and homogeneous surface of GO sheets [39]. The introduction of GO with its oxygen-containing functional groups onto PUF was verified using Fourier transform infrared (FT-IR) and X-ray photoelectron spectroscopy (XPS). The vital role of GO was verified in enhanced detection signals (Figure 2C). Moreover, the incorporation of GO reduced the maximum strain of the PUF, enabling enhanced flexibility and stretchability of the material, which make it suitable for flexible biosensors that require both biocompatibility and electroconductivity [39]. Utilizing the abundant hydrophilic groups of GO, Zhang and colleagues fabricated GO/silk fibroin (SF) with a hygroscopic LiBr gel matrix, which showed a strong correlation between the output current and humidity levels, leading to remarkable sensitivity (0.09 µA/s/1%), swift response time (1.05 s), and rapid recovery (0.80 s) [31]. As the obtained device was sensitive to humidity, it was set to respond to different respiratory frequencies simulating the relaxed, normal, and exercise states of humans, which showed totally different signal lineshapes (Figure 2D). Moreover, leveraging the capabilities of GO/SF sensors, an exceptionally integrated all-in-one respiratory monitoring–diagnosing–treatment system was developed, which allowed for the real-time collection of respiratory data and transmission through wireless networks to centralized platforms. These multifunctional humidity sensors could be used for telemedicine, the treatment of sleep apnea syndrome, or human–machine interaction (Figure 2D), inspiring new pathways for designing and fabricating power-free devices for portable and wearable applications [31]. Incorporated with other metal-based materials, sensing devices can present unique properties. A quartz crystal microbalance (QCM) humidity sensor was based on Cu(OH)$_2$ nanowires/GO composites according to the in situ growing and drop-casting method (Figure 2E). Scanning electron microscopy (SEM) images revealed the successful combination in which GO was scattered on the Cu(OH)$_2$ nanowires like a transparent mesh and still maintained its crumpled shape. The synergetic effect of Cu(OH)$_2$ and GO was verified by their enhanced sensing performance against humidity, which was further used for respiratory monitoring [40].

rGO has remarkable inherent characteristics that make it an ideal material for various applications. Notably, it demonstrates remarkable stability, boasting a large theoretical specific surface area and featuring structural defects on its surface. These distinctive features empower rGO to provide a plethora of binding sites for efficient gas adsorption [47,48]. However, the employment of chemoresistive sensor-based single-phase rGO is generally limited due to its considerable recovery time and poor selectivity because of its weak van der Waals interactions with gas molecules [49]. Therefore, Bi et al. [41] reported a self-assembled rGO-PPy composite associated with sodium alginate fabric (SA) using π-π stacking and electrostatic interaction (Figure 2F). The optimal loading rate of rGO (5 mg·mL^{-1}) ensured the sensing of NH$_3$ at low concentrations (2–16 ppm). The synergistic

effect of PPy and rGO contributed to an extraordinary sensing response of 10.7%, reaching a minimal detection limit of 2 ppm. The durability of the composites was tested, including tests of tensile strength (95.48 MPa breaking strength) and thermal stability. With its contributions of flexibility and Joule heating ability (42.4 °C, 3 V) under a safe range for human beings, rGO-PPy was ideal for practical usage in closed-loop drug delivering systems (Figure 2F) [41]. Another example was the incorporation of P-type rGO and N-type WS_2, both with 2D layered structures, for improving humidity-sensing abilities due to the abundant oxygen-containing functional groups in rGO and the regulation of electron transfer between the P-N heterointerface. Raman spectroscopy was conducted to characterize the interactions between H_2O and sensing materials, the result of which showed a distinguishable shift in the A_{1g} peak of WS_2 and rGO, which revealed the water molecules' absorption and the electron transfer to rGO. Based on their high sensitivity and quick recovery time, P-N WS_2-rGO humidity sensors were applied for the recognition of voice patterns. By evaluating the moisture content patterns in the breath during speech, the sensor demonstrated the capability to discern distinct voice signatures emanating from people's mouths (Figure 2G) [42].

　　Among the numerous modification approaches available, heteroatom doping stands out as an important method for regulating the electronic structure and introducing additional active sites to the inert lattice plane of graphene, which are highly important in multifunctional devices [50]. The introduction of a dopant atom can result in the creation of numerous active sites in graphene. In fact, a dopant atom with the distinct electronegativity of "C" disrupts the electroneutrality in graphene and generates unbalanced locally charged regions, serving as active sites within the graphene structure. Moreover, unpaired electrons in dopants give rise to a localized distribution of molecular orbitals, enhancing the chemical reactivity of graphene. Additionally, active sites can be perceived as structural flaws that arise from the disparity in size and consequent lattice strain in graphene [51]. Taking into account electronegativity, the size of the doping atoms, etc., boron-, nitrogen-, sulfur-, and phosphorus-doped graphene have been reported for different specific applications. Figure 3 [50] shows a typical chemical model of N-doped graphene, with the doping sites of N atoms in different chemical environments, whose effects on the sensing process could be distinct.
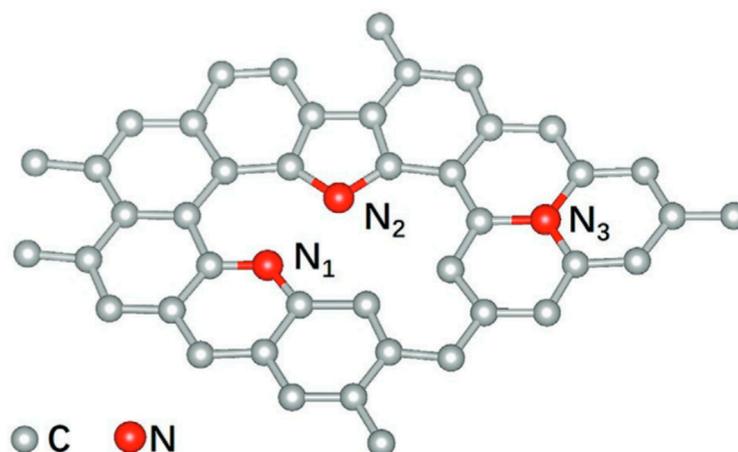

Figure 3. Schematic diagram of the atomic structure of NG. N_1, N_2, and N_3 represent pyridinic, pyrrolic, and graphitic nitrogen atoms, respectively. (Reproduced with permission from [50]. Copyright 2021, Wiley-VCH).

2.2. Transition Metal Dichalcogenides (TMDs)

　　In the 2D realm, transition metal dichalcogenides (TMDs) display versatile chemistry and tunable size-related electronic structures with variable 1–2 eV bandgaps [52,53]. For instance, bulk MoS_2 exhibits an indirect bandgap of 1.3 eV, while a direct bandgap of 1.8 eV is formed in its monolayer form [54]. Atomically thin 2D TMDs typically have a

formula of MX_2, where M represents a transition metal atom and X denotes a chalcogen atom (such as S, Se, or Te), comprising approximately 60 members [55]. In the X-M-X structure, the sulfur group element's atomic layer is sandwiched between layers of metal atoms, giving rise to a structure reminiscent of two hexagonal plane layers [56]. Depending on their chemical composition and structural combinations, these materials exhibit a wide range of properties, spanning from semiconducting behavior (e.g., MoS_2, WS_2) to semimetallic properties (e.g., WTe_2, $TiSe_2$), metallic characteristics (e.g., NbS_2, VSe_2), and even superconductivity (e.g., $NbSe_2$, TaS_2) [57]. Due to their unique properties, for example, tunable bandgaps, strong exciton binding energy, and photoluminescence properties, TMDs have been widely used in photodetectors. Moreover, in the gas-sensing field, one of the most intriguing characteristics of TMD sensors lies in their remarkable ability to detect gas molecules at room temperature (RT), owing to the distinctive electronic properties derived from their atomically thin 2D structure [16]. Recent advancements have demonstrated that the creation of heterostructures serves as an effective approach to manipulating the sensing properties of TMD materials (Table 2); combining them together with other functional materials makes TMD-based devices potential candidates for multifunctional sensors.

Table 2. Summary of TMD-based multifunctional gas sensors.

Sensing Materials	Target Gas	Other Functions	Ref.
MoS_2/SnO_2	Trimethylamine	• Fantastic gas sensing • Catalytic reduction property	[58]
Li-2D WS_2	NH_3	• Distinguishes between bending and gas response signals at the same time	[59]
VA-2D MoS_2	NO_2	• Large lateral stretchability	[60]
n-WS_2/p-GeSe/n-WS_2	NH_3, O_2	• Electrical transistor	[61]
g-C_4N_3/MoS_2	NO, etc.	• Spin filtering	[62]
WSe_2 nanosheets	Triethylamine, NO_2	• Selective sensing under UV illumination	[63]
SnS_2 quantum dot	NO_2	• Photodetection	[64]
LIG/MoS_2	NO_2	• Heater operation • Acoustic alarm	[65]
NbS_2-Nb_2O_5-NbS_2	Humidity	• Temperature sensor • NH_3 sensor	[66]
$PtSe_2$	NH_3	• Wireless wearable molecule detection circuits	[67]

It is well known that the fabrication of atomic precise heterostructures requires advanced instruments, which is time-consuming and difficult with large-scale production, hindering their practical applications. Therefore, the development of in situ nondestructive processing methods for the preparation of TMD-based heterostructures is of great urgency. Liu et al. [66] reported a laser patterning method for direct oxidation of metallic NbS_2 into Nb_2O_5, forming a NbS_2-Nb_2O_5-NbS_2 heterostructure which was constructed with a remarkable configuration, featuring an ultrathin Nb_2O_5 channel with both ends connected to two metallic TMD (NbS_2) electrodes. This ingenious design ensures the formation of

naturally perfect interface contacts, ensuring robust electrical signals in a two-terminal sensor. Due to the effective modulation of Nb_2O_5 surface conduction, the NbS_2-Nb_2O_5-NbS_2 heterostructure exhibits exceptional sensitivity in detecting temperature, humidity, and NH3. The positive temperature coefficient of resistance of these sensors can reach an impressive range of 15–20% per degree Celsius. In a humid environment, the electrical conductance undergoes a significant change of approximately three orders of magnitude as the relative humidity (RH) fluctuates from 30% to 90%. Moreover, the sensitivity ($\Delta R/R$) of NH_3 at a concentration of 50 ppm reaches an outstanding level of 80%, accompanied by a low detection limit of 1 ppm. The fabrication of flexible devices on a PET substrate was feasible despite the fragile characteristics of Nb_2O_5 ceramic due to the small thickness of the heterostructure (Figure 4). During the bending test, the electrical conductivity of our flexible device demonstrated remarkable stability, with minimal changes observed even at bending radii as low as 3 mm. Furthermore, the device retains its performance after undergoing 200 bending cycles at a bending radius of 10 mm, thus highlighting its exceptional flexibility and reliability (Figure 4) [66].
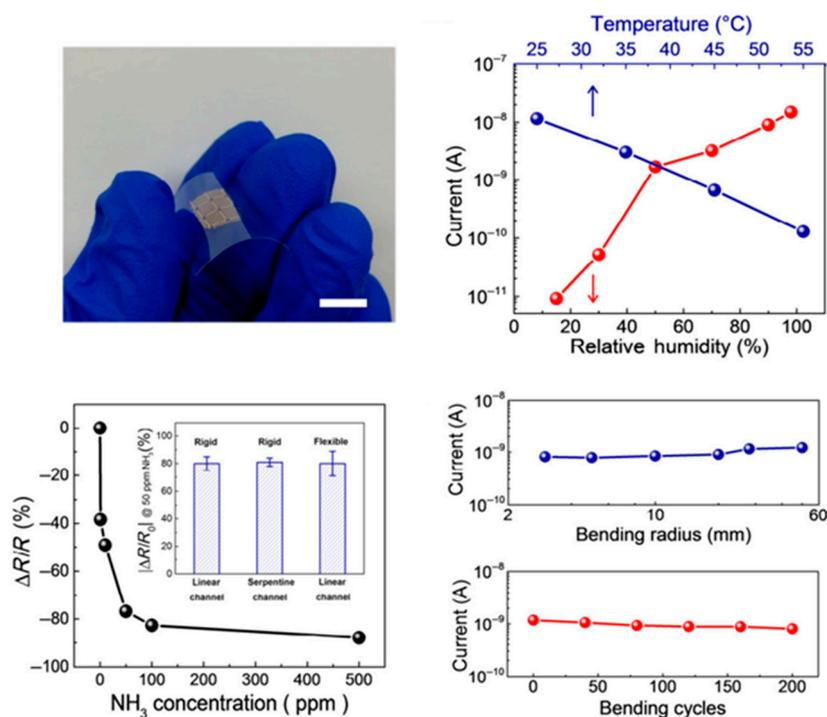

Figure 4. Flexible NbS_2-Nb2O_5-NbS_2 sensors. Photographs of flexible device and corresponding humidity-, temperature-, and NH_3-sensing performance. (Reproduced with permission from [66]. Copyright 2020, Springer).

Strain engineering has garnered considerable attention due to its vast potential in manipulating the electrical, optoelectronic, magnetic, and electrochemical properties of TMDs, black phosphorus, and other 2D materials [57,68]. A strain-enhanced $PtSe_2$ wireless wearable gas sensor was fabricated for the ultrasensitive detection of trace NH_3 [67].

$PtSe_2$ nanosheets were directly grown on a polyimide substrate and subsequently integrated with spiral interdigital electrodes, offering distinct advantages over traditional parallel interdigital electrodes and resulting in a more effective sensing area, thereby significantly enhancing the accuracy of the sensors. Real-time sensing tests demonstrated a significant enhancement in the sensitivity of $PtSe_2$, reaching 31.67% ppm^{-1} at a strain curvature of 1/4 mm^{-1}, which was approximately 300% higher than the flat state. The mechanism behind this enhancement was attributed to the distortion of the horizontal lattice of $PtSe_2$ with strain, which resulted in a decrease in adsorption energy. The wireless sensing platform, incorporating a Bluetooth module, ensured seamless real-time monitoring

with cloud server support, which could prove to be invaluable for various healthcare and industrial applications (Figure 5). The system exhibited remarkable consistency in maintaining high sensitivity and stability even in low-concentration ranges of molecule detection. Notably, it showcased average responses of 11.2% and 27.3% in five cycles at 1 and 5 ppm, respectively, underscoring its exceptional performance in detecting and monitoring trace gas concentrations. Additionally, the data fluctuations remained within a minimal range of 10%, further emphasizing the system's reliability [67].
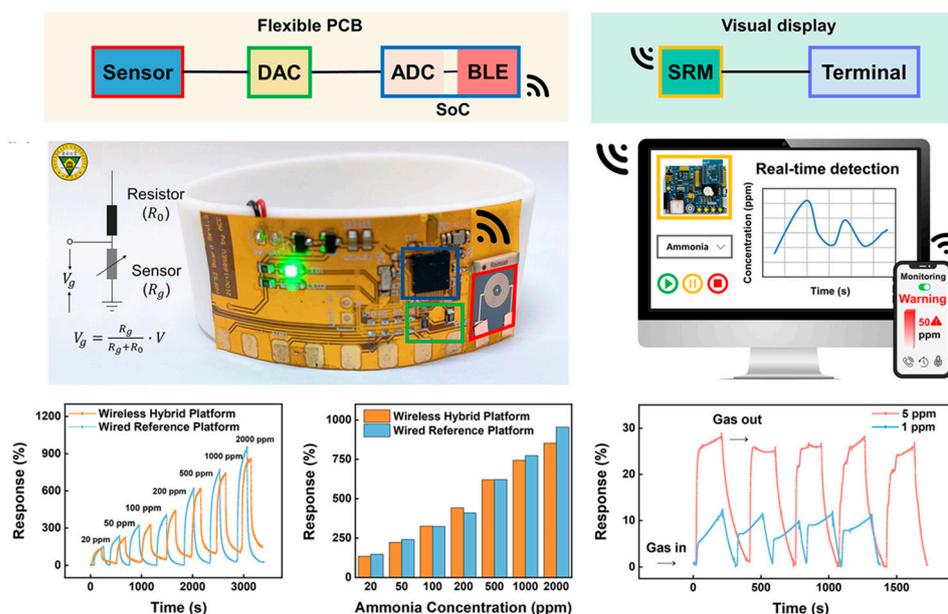

Figure 5. Circuit design and wireless sensing of ammonia performance of PtSe$_2$ gas sensor. (Reproduced with permission from [67]. Copyright 2023, American Chemical Society).

2.3. MXenes

MXenes represent a diverse family of 2D compounds comprising metal carbides, nitrides, and carbonitrides, exhibiting a unique architecture characterized by the arrangement of two or more layers of a transition metal (M atoms) in a honeycomb-like lattice. These M layers are interleaved with carbon and/or nitrogen layers (X atoms), which occupy the octahedral sites situated between the adjoining transition metal layers [69]. In the last decade, MXene materials have experienced a remarkable expansion, owing to their exceptional electrical, mechanical, and chemical properties derived from their distinctive 2D structure. MXenes are usually represented by the equation $M_{n+1}X_nT_x$ (n = 1–4); M and X are transition metals and contain C/N as mentioned above, and Tx is regarded as a surface terminal group (O/OH/F/S and Cl), featuring a unique combination of metallic conductivity and colloidal processability [70]. Over 70 MAX phases and more than 30 distinct stoichiometric forms of MXenes have already been discovered, with numerous additional ones predicted to exist [71]. Gas sensors based on MXenes exhibit excellent capabilities in detecting volatile organic compounds (VOCs) and nonpolar gases, including ammonia, ethanol, and acetone, even at room temperature. This remarkable sensitivity can be attributed to their metallic core channels and surface functional groups, which contribute to the formation of strong adsorption energies for these specific gas molecules [69]. Attributed to the moderate mechanical strength of MXenes (M-X bonds endow a high elastic constant that exceeds 500 GPa) [18], when incorporating flexible substrates, MXenes open up a wide range of practical applications involving flexible multifunctional sensing devices (Table 3).

Table 3. Summary of MXene-based multifunctional gas sensors.

Sensing Materials	Target Gas	Other Functions	Ref.
MXene/WO_3	NO_2	• Detection of wind direction • Wind-driven and self-powered	[72]
Au/HT-Nb_2CT_x	NH_3	• Monitoring NH_3/temperature/humidity in a hog house and vegetable greenhouse	[73]
MXene/CuO	NH_3	• Self-powered wearable device for body movement detection	[74]
$Ti_3C_2T_x$/NH_2-MWCNTs	Formaldehyde	• Self-powered respiratory detection	[75]
Porous crumpled MXene spheres	NO_2	• Wearable pressure sensor	[9]
CeO_2/V_2C	NH_3	• Detection of industrial water	[76]
MXene/TiO_2/cellulose	NH_3	• Self-powered insole	[77]
MXene/silver nanowire/silk textiles	Humidity	• Electromagnetic interference shielding	[78]
β-Ni(OH)$_2$/MXene	Ethanol	• Self-powered alarm system	[79]
Cellulose/$Ti_3C_2T_x$	NH_3	• Pressure-sensing ability • Oral healthcare	[80]
$Ti_3C_2T_x$ fabric	Humidity	• Joule heating • Thermotherapy • Bacterial ablation and wound healing	[81]

Since the invention of the triboelectric nanogenerator (TENG) by Wang and colleagues in 2012 [82], self-powered flexible devices have emerged rapidly based on TENGs. Numerous studies have demonstrated the effectiveness of TENGs in enhancing gas-sensing performance and reducing power consumption in gas sensors, especially with MXenes as the sensing materials that could operate at low-power consumption of mW to μW. For instance, Wang et al. [72] successfully developed a gas sensor using $Ti_3C_2T_x$/WO_3, which exhibited a notable response to NO_2 gas stimulation at room temperature (Figure 6A). VOCs are prevalent air pollutants known for their toxicity to humans. Therefore, it is of the utmost importance to detect VOCs rapidly, selectively, sensitively, and reversibly. When airborne VOCs interact with a gas sensor, the sensing layer undergoes a resistance change as the volatile gas reacts with the sensing layer, representing the primary mechanism behind gas sensor formation. Poly(vinyl alcohol)/silver (PVA/Ag) nanofibers are a high-performance TENG material, showing an output voltage of 530 V and power of 359 mW/m^2. For a practical TENG device with a smaller size ($1 \times 2 \times 3$ cm^3), a real-time test indicated that the prepared breath-driven TENG could differentiate various respiratory behaviors, making it highly promising for respiratory monitoring applications (Figure 6A). Further efforts were made for its biocompatibility for monitoring human movement and harvesting human kinetic energy, and it successfully distinguished different movements (elbow bend, knee bend, and foot movement) based on voltage outputs (Figure 6A). This TENG-based $Ti_3C_2T_x$/WO_3 gas sensor showed promising abilities in NO_2 sensing, with an excellent response (~510%) at room temperature that was 15 times larger than that of the resistive sensor [72].
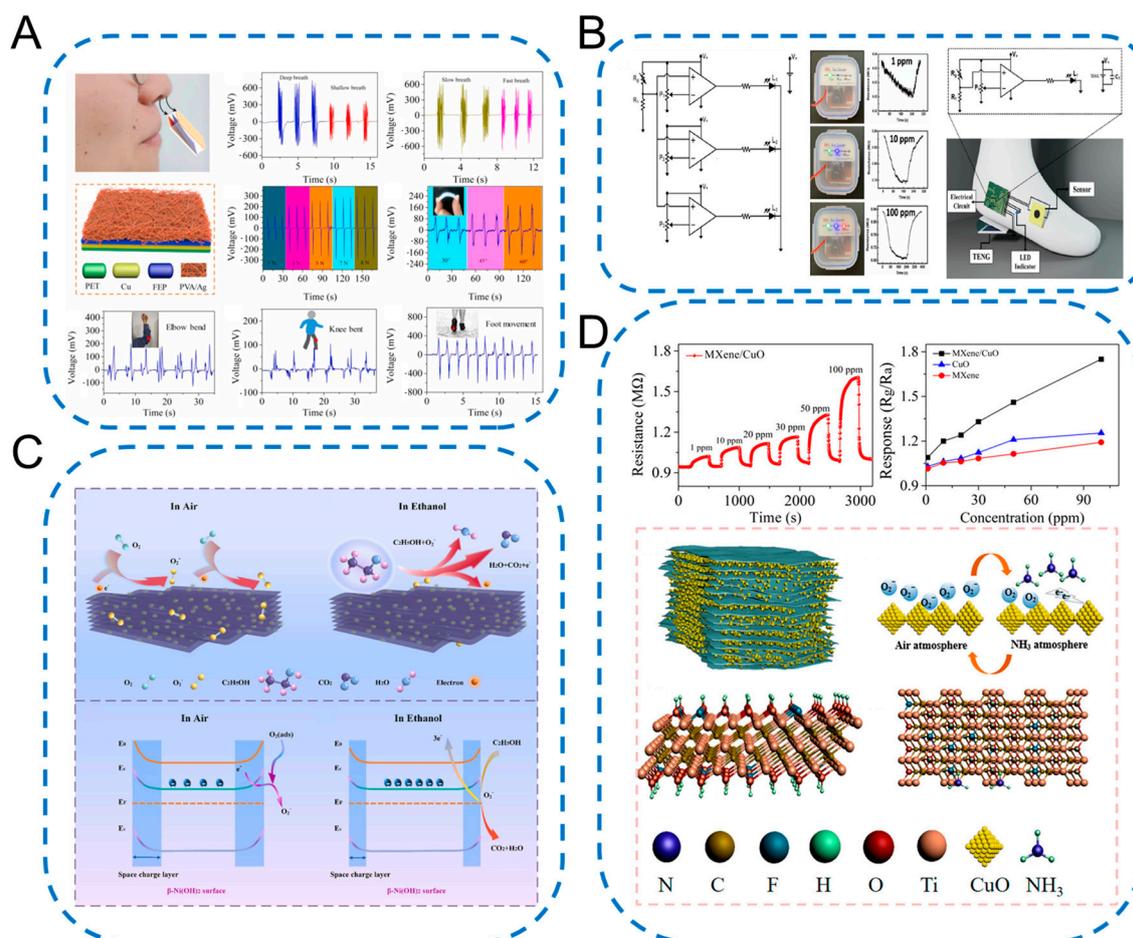
Figure 6. MXene-based self-powered multifunctional gas sensors. (**A**) Properties of MXene/WO$_3$ triboelectric nanogenerators (TENGs) with different respiratory intensities/frequencies and angles. (Reproduced with permission from [72]. Copyright 2021, Elsevier). (**B**) MXene/TiO$_2$/cellulose gas monitoring device with an LED display. (Reproduced with permission from [77]. Copyright 2022, American Chemical Society). (**C**) Schematic of the sensing mechanism/energy band structure of the β-Ni(OH)$_2$/MXene hybrid. (Reproduced with permission from [79]. Copyright 2023, Elsevier). (**D**) The dynamic resistance test of the MXene/CuO sensor exposed to various NH$_3$ gas concentrations and corresponding possible sensing mechanism. (Reproduced with permission from [74]. Copyright 2021, American Chemical Society).

Similarly, different conducting polymers were used in TENG-based gas sensors. A MXene/cellulose acetate NFs (MXene/CA-NFs) combination was synthesized [77], with MXene as the negative layer and CA-NFs as the positive layer, with resulting high output power (~1361 mW/m^2@2 MΩ). The sensing material consisted of a MXene/TiO$_2$ heterostructure, exhibiting selective detection of NH$_3$ with a high response (6.84%, 10 ppm). In this context, the electron-enriched TiO$_2$ acted as a catalyst, effectively attracting oxygen molecules to its surface and promoting the absorption of additional O$_2^-$ anions. Simultaneously, MXene served as a selective matrix for NH$_3$, facilitating the interaction between NH$_3$ and the preadsorbed O$_2^-$ anions. Furthermore, the conductive channel provided by MXene contributed to the overall reduction in resistance within the heterojunction sample, thereby accelerating the redox reaction even at room temperature. A self-powered NH$_3$ sensor was embedded in the insoles of shoes to automate NH$_3$ detection (Figure 6B), which could be conducted with gentle shoe tapping in ambient conditions, and with NH$_3$ causing an integrated LED to light up [77]. In this situation, MXenes were used both as TENG and sensing materials, indicating their multifunctional properties. Aside from the combination with metal oxides, the MXene-based heterostructure also showed an enhanced sensing

ability for ethanol and NH3 with β-Ni(OH)$_2$ and MOF derivates, showing a similar sensing mechanism with more O_2^- generation (Figure 6C,D).

The development of gas sensors is of great importance for monitoring exhaled breath, body fluids, and humidity, which makes it useful in early disease diagnosis and further treatment. Therefore, MXene-based gas sensors for healthcare are now receiving a great amount of attention. Zhao et al. [81] (Figure 7) reported a Ti$_3$C$_2$T$_x$ MXene fabric (M-fabric) with a fast humidity response (1.15 s response time, 8.71 s recovery time) with stability for more than 25 days which is potentially suitable for monitoring exhalation changes in patients. The same M-fabric also showed Joule heating ability and could reach 100 °C under 6 V input voltage within 16 s, allowing for application in personal thermal management devices. In fact, heat generated by M-fabric wearable thermal management devices could diffuse along the skin and muscle, which is beneficial for pain relief (Figure 7). Moreover, the Joule heating ability of M-fabric was also applied in bacterial ablation and infectious healing, exhibiting efficient elimination of *S. aureus* bacterial infection with almost 100% reparation of trauma (Figure 7) and without obvious organ damage [81]. Aside from wound treatment, dental diseases could also be evaluated by monitoring the release of specific gases like CH$_3$SH, H$_2$S, and NH$_3$ in oral medicine. Therefore, Jin et al. [80] reported a cellulose/Ti$_3$C$_2$T$_x$ MXene bioaerogel that could not only realize real-time multipoint detection of occlusal force but also the oral release of NH$_3$. A small device (6 × 6 cm^2) containing a 17 × 17 pixel array that is suitable for the human mouth was designed and fabricated, and could record in real time the intensity, contact position, shape, and force distribution of tooth contact. At the same time, cellulose/Ti3C2Tx MXene could distinguish between bite force signals and the NH$_3$ gas signal, suggesting a multifunctional sensing platform that could help with clinical diagnosis of undetectable dental lesions. Interestingly, the cellulose/Ti3C2Tx MXene bioaerogel was degradable with 2 wt.% H$_2$O$_2$ in 10 min, further demonstrating its usefulness in practical dental diagnosis [80]. MXene-based sensors have also shown the probability of application in noninvasive disease diagnosis via urinary volatiles [83], electromagnetic interference shielding [78], etc.
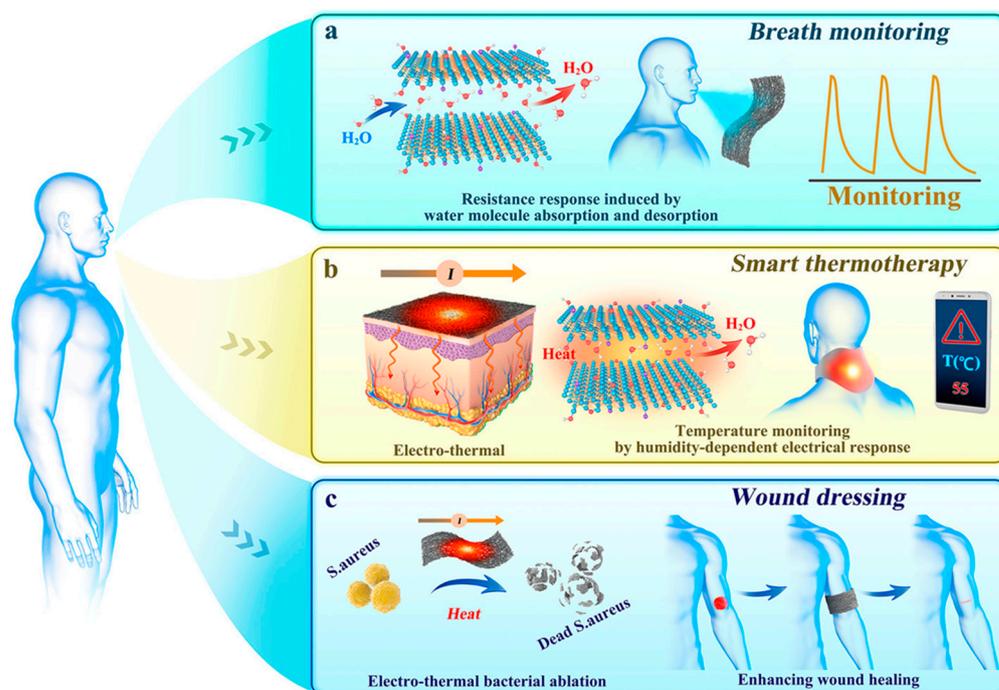

Figure 7. Schematic illustration of flexible and wearable MXene-based devices, including breath monitoring, thermotherapy, and bacterial ablation devices. (Reproduced with permission from [81]. Copyright 2020, American Chemical Society).

2.4. Other 2D Materials

Aside from the aforementioned materials, other 2D materials, such as black phosphorous (BP) [84], 2D metal–organic frameworks (MOFs) [85,86], graphitic carbon nitride (g-C_3N_4) [87–92], etc., have been obtained and characterized as thin layered nanostructures which showed superior ability in gas sensing (Table 4). The diverse and distinctive electronic, physical, and chemical properties exhibited by two-dimensional materials, resulting from the confinement of electronic and magnetic states, have led to remarkable advancements.

Two-dimensional MOFs, in contrast to most two-dimensional materials, have an inherent porosity that offers advantages in terms of analyte absorption into the material and presents distinctive avenues for surface interactions that are not accessible in nonporous two-dimensional materials. Furthermore, the structural modularity of MOFs, which can be achieved through the use of synthetically tunable molecular building blocks, enables precise customization of host–guest interactions embedded within the scaffold [93]. Smith et al. successfully integrated 2D conductive MOFs, specifically M_3HHTP_2 (where M represents Ni and Cu), into polymeric device chips that were equipped with prepatterned graphitic electrodes. The outcome of this process was the formation of mats comprising randomly oriented MOF nanowires, which had a thickness of approximately 15 μm. The resulting devices exhibited promising performance in distinguishing between gas-phase NH_3, NO, and H_2S at concentrations ranging from 10 to 80 ppm [85]. MOF-based multifunctional electrically conductive textiles were also fabricated using direct solution-phase growth of Ni_3HHTP_2 and Ni_3HITP_2 MOFs on flexible fabric-based substrates. This innovative approach, termed self-organized frameworks on textiles (SOFT), leveraged the porosity of both the MOF and the fabric, resulting in textiles with excellent mechanical stability. The SOFT sensors exhibited remarkable capabilities as they were able to simultaneously detect, capture, and filter NO and H_2S gases with sub ppm limits of detection (0.16 ppm for NO and 0.23 ppm for H_2S) [86]. Importantly, the chemiresistive response of the SOFT sensors remained largely unaffected by the presence of humidity (18% relative humidity) and could be fully recovered by washing with water [86].

Table 4. Summary of other multifunctional gas sensors.

Sensing Materials	Target Gas	Other Functions	Ref.
BPNS-PEI-TPPS	HCl, NH_3	• Surface-enhanced Raman scattering	[84]
2D M_3HHTP_2	NH3, NO, H_2S	• Distinguishing different gases	[85]
2D Ni_3HHTP_2 2D Ni_3HITP_2	NO, H_2S	• Detecting, capturing, and filtering gas simultaneously	[86]
$MoSi_2As_4$	NH_3, NO_2	• FET integration switching	[94]
Au-InSe	NH_3, NO_2	• Wearable measurement system	[95]
g-C_3N_4-Fe-Cu	Methane	• Humidity detection • Soil moisture content detection	[88]
Au–TiO_2-g-C_3N_4	VOAs	• Photocatalyst	[89]
Nb-doped g-C_3N_4	NH_3	• Photocatalyst	[90]
ZnO/Ag/g-C_3N_4	NO_2	• Photocatalyst	[91]
CeO_2/g-C_3N_4	Humidity	• Human physiological detection	[92]
g-C_3N_4/GaN	NO_2	• UV photodetector	[87]

Graphitic carbon nitride (g-C_3N_4) is a metal-free semiconductor composed of carbon and nitrogen, two elements abundant in the Earth's crust. This material exhibits visible-light activity, possessing a bandgap of approximately 2.7 eV (corresponding to a wavelength of around 460 nm). Thanks to its exceptional optical properties of effective light harvesting, g-C_3N_4 has found wide application as a photocatalyst for processes such as water splitting, pollution degradation, and CO_2 reduction. In terms of gas sensing, g-C_3N_4 boasts an intrinsic crystal structure reminiscent of 2D layered graphite materials, which imparts it with fascinating physicochemical properties, a unique electronic structure, and remarkable chemical stability. When exposed to light irradiation, g-C_3N_4 demonstrates an augmented adsorption capacity for various gases, consequently enhancing its sensing capabilities. Khasim et al. [88] successfully synthesized composites of g-C_3N_4 filled with FeO and CuO, which showed superior methane sensing ability at the ppb level, with high sensitivity, short response/recovery times, and long-term stability. The presence of amino groups in g-C_3N_4 led to hydrogen bonding and continuously binding with water molecules, verifying its humidity-sensing performance. The synthesized composites were utilized for the practical detection of water content in soil samples, yielding responses of 72% for black clay soil and 59% for red garden soil. These results highlight the suitability of these composites as ideal platforms for monitoring diverse greenhouse conditions and agricultural applications [88]. g-C_3N_4 is an excellent photocatalyst, and integrating its photocatalytic capability with its gas-sensing ability in a single device enables the realization of multifunctionality in one single device, with potentially enhanced gas-sensing performance under light irradiation conditions. Malik et al. [89] reported an Au–TiO_2-g-C_3N_4 nanohybrid which exhibited enhanced photocatalytic degradation performance toward a variety of azo dyes due to its superior ability to generate superoxide anionic free radicals. Similarly, when molecular oxygen trapped electrons in the conduction band of TiO_2 and g-C_3N_4, this resulted in the creation of reactive oxygen species, which was responsible for the activation of gas molecules. The sensing tests confirmed the proposed mechanism, with excellent sensing performance toward the volatile organic amines (VOAs) commonly present in the indoor climate [89]. For other gases, like NO_2 [91] and NH_3 [90], the enhanced sensing properties of g-C_3N_4 were also shown, indicating its universality as a gas sensor. Moreover, like other 2D materials, g-C_3N_4 could serve as a highly flexible sensor for detection of human body physiological information [92].

As sensing materials, 2D materials exhibit different sensing mechanisms and demonstrate diverse sensing capabilities due to their various structural types and their responsiveness to different types of gases. The underlying principle of the vast majority of gas sensors is based on the interaction between gas molecules and the sensing material, which leads to changes in the physical and chemical properties of the sensing material, including in chemiresistive, colorimetric, electrochemical, surface acoustic wave, and magnetic sensors, enabling gas detection. The most widely recognized sensing mechanisms for 2D materials are the surface-adsorbed oxygen ion mechanism and the charge-transfer mechanism. For example, as mentioned before, most modified graphene-based materials reveal p-type semiconductor behavior, showing a tendency to adsorb O_2 and H_2O molecules in air [22]. In the case of oxidizing gases such as NO_2, SO_2, and Cl_2, which possess electron-withdrawing abilities, the concentration of the primary charge carriers (holes) on graphene increases due to the decrease in electron concentration. Consequently, the conductivity of the graphene-based sensor improves, manifesting the sensing signal as a reduction in resistance. Similarly, in other 2D materials, when exposed to various gases, the sensing materials undergo charge-transfer reactions with the adsorbed gases, resulting in different directions and quantities of charge transfer, leading to varying changes in the materials' resistance. This mechanism can reasonably explain sensing phenomena in materials such as TMDs, graphene and its derivatives, and MXenes. Efforts have been made with the fabrication of different kinds of junctions (Schottky junctions, and p–n, n–n, and p–p junctions), which focuses on the modulation of band structures and interfacial charge-transfer characteristics. Another important sensing mechanism, which is called the

surface-adsorbed oxygen ion mechanism, often requires adsorption of negative oxygen ions on the surface of metal oxides, especially in oxygen vacancies or other defects on the surface of 2D materials [96,97].

In recent decades, the combination of different materials and the formation of composite structures have resulted in a combination of detection principles. Table 5 lists representative 2D sensing materials (including composites with 2D materials) for the detection of different gases with performance differences, from which one can conclude that designing sensors with high sensitivity and selectivity against specific gas molecules requires precise selection of sensing materials, defect engineering, and interface engineering [96,97].

Table 5. Summary of representative 2D sensing materials and corresponding performance.

Sensing Materials	Target Gas	LOD	Response ($\Delta R/R_a$)	Mechanism	Ref.
PS/graphene	50 ppm NO_2	4.8 ppb	45.1%	Charge transfer	[98]
GO	800 ppm CO_2	4.75 ppm	75.4%	Charge transfer	[99]
SnO_2/rGO/PANI	0.1 ppm H_2S	0.05 ppm	9.1%	Surface-adsorbed oxygen ions Charge transfer	[100]
$PtSe_2$	1 ppm NO_2	0.2 ppb	600%	Charge transfer	[101]
$PtSe_2$	NH_3	50 ppb	29.98%	Charge transfer	[67]
MoS_2/graphene	NO_2	14 ppb	90%	Charge transfer	[102]
$Ti_3C_2T_x$/WSe_2	40 ppm ethanol	-	9.2%	Surface-adsorbed oxygen ions Charge transfer	[103]
V_2CT_x	100 ppm H_2	2 ppm	0.22	Charge transfer	[104]
Cellulose/$Ti_3C_2T_x$	NH_3	-	6.0%	Charge transfer	[80]
InSe	1 ppm NO_2	0.98 ppb	100%	Charge carrier transfer Schottky barrier modulation	[105]
BP–In_2O_3	100 ppb NO_2	10 ppb	12	Surface-adsorbed oxygen ions Charge transfer	[106]
g-C_3N_4/CuO	Acetone	10 ppb	143.7 (R_g/R_a)	Surface-adsorbed oxygen ions Charge transfer	[107]

LOD represents the limitation of detection, R_g represents resistance in presence of target gases, and R_a represents the resistance in air.

3. Smart Gas Sensors for Artificial Intelligence

The human body is an extraordinary integrated system that boasts numerous captivating design features. Taking inspiration from these remarkable qualities, a diverse range of functional devices have already been developed and implemented in the form of flexible intelligent robots, including optoelectronics for computer vision, electronic skin for machine touch, and versatile algorithms for speech recognition. With this backdrop, there is a growing demand for the development of a flexible and intelligent electronic nose (e-nose), which, thus far, remains unexplored territory [108]. Emerging technologies, together with advancements in artificial intelligence (AI) subdivisions such as robotics, deep learning (DL), and machine learning (ML), have paved the way for the development of novel techniques for food quality control, disease diagnosis, and explosive detection [109]. With the help of DL and ML, predictions on sensing materials about their structure, physicochemical properties, and stability could be conducted [110,111], together with simulation and visualization without conducting real experiments. Moreover, AI and ML tools have firmly discarded the anticipation-based hit–trial strategies and upgraded data analysis and reasoning-based sensing studies.

For example, Wan et al. [112] reported a state-of-the-art DFT and ML hybrid scheme for the accessibility analysis of transition metal (TM)/g-C_3N_4 heterostructures. The research was entirely based on computational simulation; at first, 28 different potential TM/g-C_3N_4

structures were predicted and modeled, followed by the bond analysis of the template analyte molecule CF_3SO_2F, indicating that CF_4, SO_2F_2, SO_2, and HF were the most energetically favorable products. Furthermore, ML was employed to investigate the interaction strength between 28 different $TM/g\text{-}C_3N_4$ structures and four decomposed products (a total of 112 combinations), which was costly with the first principal calculations. The ML workflow is depicted in Figure 8 [112]; an adsorption model of 28 randomly selected gas-$TM/g\text{-}C_3N_4$ systems was first studied using DFT calculations, followed by feature generation, engineering, model training and testing, model selection, and finally, model prediction. The 84 ML-predicted adsorption energies ranged from -2.84 to -0.05 eV, showing no obvious changing tendency with the change in the TM atom, indicating the dual influence of the TM atom and decomposition gases on interaction strength. Based on the ML-predicted adsorption energy, a high-throughput screening process for parameters like recovery time, sensitivity, selectivity, and stability was conducted. Finally, four promising gas-sensing materials, $Sc/g\text{-}C_3N_4$, $Pd/g\text{-}C_3N_4$, $Zn/g\text{-}C_3N_4$, and $Cd/g\text{-}C3N4$ for CF_4, HF, SO_2, and SO_2F_2, respectively, were determined [112]. Another significant application for AI is to distinguish different components in mixed gases. By extracting features from the sensing data of a single specific gas component and modeling, even though the sensing data of the mixture were totally different and complex, one could classify each component with ML, indicating its practical application in gas sensing in different work conditions [113,114]. Herein, we only propose and emphasize the importance of AI-based smart gas sensors, rather than going into detail about specific scientific issues in computer science. The initial conditions of the ML process in the presented literature are summarized in Table 6. It is emphasized that for readers interested in more detailed coding and algorithms, milestone works have already been reviewed [115,116].
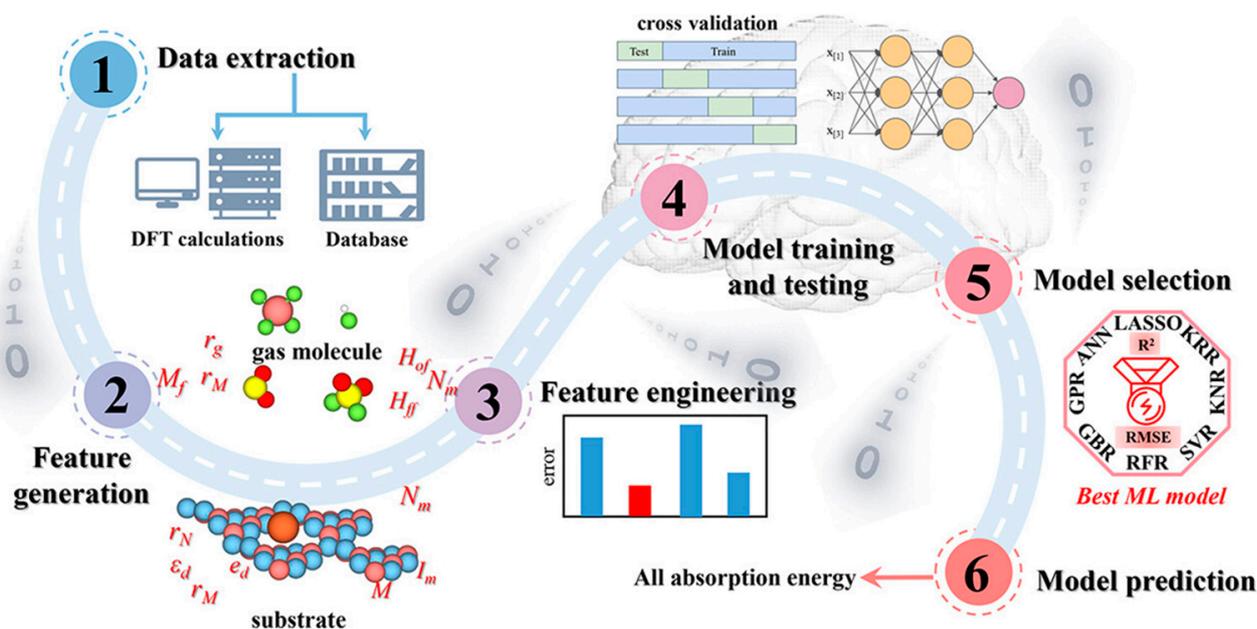

Figure 8. Machine learning workflow for investigating the interaction strength of all possibilities between 4 CF_3SO_2F decomposed gas products and 28 $TM/g\text{-}C_3N_4$ structures with common ML algorithms. (Reproduced with permission from [112]. Copyright 2023, American Chemical Society).

Table 6. Initial conditions of ML process in the presented literature.

Sensing Materials	Target Gas	Features	Data	Model	Ref.
TM/g-C$_3$N$_4$	CF$_3$SO$_2$F	TM atoms (radius, relative mass, electron number of the outmost d orbital, etc.) Adsorption atoms Gas molecules (Total 21 features)	28 random models	8 different algorithms	[112]
GeS	VOCs	Current changes Time difference (Total 3 features)	10 measurements for each VOC	Bayes classifier	[113]
Graphene-CuPc	NH$_3$	$_{a1}$, b_1, c_1, k_{max}, area, etc. (Total 11 features)	24 individual measurement profiles	L2 norm	[114]

4. Conclusions and Outlook

We have summarized the current research on multifunctional gas sensors based on 2D materials with varieties of different applications, such as motion detection used in respiratory monitoring, photodetection, catalysts, temperature sensing, pressure sensing, human healthcare, etc. Utilizing the unique physical and chemical properties of different kinds of 2D materials, self-powered, low-energy-consuming, human-suitable wearable smart devices have been the most attractive research topic and many breakthroughs have already been made. In this review, we first summarized the multifunctional gas sensors based on graphene and its derivates, including GO, rGO, and doped graphene. As one of the largest kinds of material in the 2D material family, graphene/GO/rGO vary in their surface chemistry due to the participation of oxygen-containing functional groups; therefore, they are suitable in diverse working conditions. Second, TMD-based multifunctional gas sensors were summarized and discussed. TMD itself is a promising material with tunable bandgaps and mechanical strength; hence, a combination of TMDs and other functional materials— sensors with different dimensions in the field of smart wearables—was fabricated and tested. Third, we discussed MXenes, which were born and developed in the last 10 years and which have metallic core channels and surface functional groups which contribute to the formation of strong adsorption energies for these specific gas molecules. The MXene-based sensors played an important role in medical healthcare monitoring. Fourth, other 2D materials such as MOFs and g-C$_3$N$_4$ with dual abilities in catalysis and gas sensing were discussed. Lastly, AI and ML techniques have been recently introduced to sensors, and could be applied for the prediction and designing of new sensing materials and complex signal processes.

Although we have listed many outstanding, noteworthy, and distinctive two-dimensional materials and their practical applications in multifunctional gas sensors in this review, there is a portion that has been overlooked, which includes other rapidly evolving families of two-dimensional materials with diverse electronic characteristics and chemical compositions. These novel 2D materials possess distinct mechanical, magnetic, electrical, and other physical properties compared with traditional materials, thereby presenting potential application capabilities in a broader range of research fields. Moreover, by using DFT calculations for the design of novel 2D materials, researchers have obtained a significant number of materials that have not yet been successfully synthesized but which also deserve attention and investigation, as some theoretical calculations have indicated their potential for outstanding performance in gas-sensing applications. Furthermore, while we have provided an overview of some representative applications of multifunctional gas sensors, the underlying physicochemical mechanisms and the design of and improvements in next-generation devices specific to each application have not been mentioned in this review, due to the complexity of the mechanisms involved in each distinct application. And we have

only focused on some of the most current and trending applications, neglecting many other areas of application. Although such achievements have already been made, due to the rapid development of the IoT platform and fifth-generation (5G) communication, the practical use of existing sensing devices out of the lab is an issue of great urgency, and some research has realized their real-time sensing and monitoring in smartphones, laptops, etc. Developments should also be made in interdisciplinary areas, for example, medical monitoring using other biomarkers and disease diagnosis in other organs, environmental detection of VOCs as pollution source, fire alarms, and energy-harvesting devices. Moreover, to improve the sensing performance, the combination of other functional materials (metal oxides, carbon nanotubes, polymers) would inevitably make the sensing mechanisms more complicated to understand, which would lead to neglecting the intrinsic abilities of these 2D materials. Therefore, the competition between sensing performance and the adding of new compounds should be balanced. Attention should be paid to these brand-new materials. It is hoped that this review can provide a clear vision for the future development of 2D material-based sensors and encourage innovative studies and practical applications of research in this area.

Author Contributions: Supervision and writing, Z.L.; writing, Z.Q.; formatting, literature survey, figure integration, and copyright acquisition, C.-Y.L.; review and editing, Y.S. All authors have read and agreed to the published version of the manuscript.

Institutional Review Board Statement: Not applicable.

Informed Consent Statement: Not applicable.

Data Availability Statement: Not applicable.

Conflicts of Interest: All authors declare no conflict of interest.

References

1. Majhi, S.M.; Mirzaei, A.; Kim, H.W.; Kim, S.S.; Kim, T.W. Recent advances in energy-saving chemiresistive gas sensors: A review. *Nano Energy* **2021**, *79*, 105369. [CrossRef]
2. Bag, A.; Lee, N.-E. Gas sensing with heterostructures based on two-dimensional nanostructured materials: A review. *J. Mater. Chem. C* **2019**, *7*, 13367–13383. [CrossRef]
3. Dai, J.; Ogbeide, O.; Macadam, N.; Sun, Q.; Yu, W.; Li, Y.; Su, B.-L.; Hasan, T.; Huang, X.; Huang, W. Printed gas sensors. *Chem. Soc. Rev.* **2020**, *49*, 1756–1789. [CrossRef]
4. Majder-Łopatka, M.; Węsierski, T.; Dmochowska, A.; Salamonowicz, Z.; Polańczyk, A. The influence of hydrogen on the indications of the electrochemical carbon monoxide sensors. *Sustainability* **2020**, *12*, 14. [CrossRef]
5. Kim, Y.; Goo, S.-G.; Lim, J.S. Multi-Gas analyzer based on tunable filter non-dispersive infrared sensor: Application to the monitoring of eco-friendly gas insulated switchgears. *Sensors* **2022**, *22*, 8662. [CrossRef]
6. Wang, X.; Qin, J.; Hu, Q.; Das, P.; Wen, P.; Zheng, S.; Zhou, F.; Feng, L.; Wu, Z.S. Multifunctional mesoporous polyaniline/graphene nanosheets for flexible planar integrated microsystem of zinc ion microbattery and gas sensor. *Small* **2022**, *18*, 2200678. [CrossRef]
7. Wang, L.; Lou, Z.; Jiang, K.; Shen, G. Bio-multifunctional smart wearable sensors for medical devices. *Adv. Intell. Syst.* **2019**, *1*, 1900040. [CrossRef]
8. Tai, H.; Wang, S.; Duan, Z.; Jiang, Y. Evolution of breath analysis based on humidity and gas sensors: Potential and challenges. *Sens. Actuators B Chem.* **2020**, *318*, 128104. [CrossRef]
9. Yang, Z.; Lv, S.; Zhang, Y.; Wang, J.; Jiang, L.; Jia, X.; Wang, C.; Yan, X.; Sun, P.; Duan, Y.; et al. Self-assembly 3D porous crumpled MXene spheres as efficient gas and pressure sensing material for transient all-MXene sensors. *Nano-Micro Lett.* **2022**, *14*, 56. [CrossRef]
10. Bag, A.; Lee, N.-E. Recent advancements in development of wearable gas sensors. *Adv. Mater. Technol.* **2021**, *6*, 2000883. [CrossRef]
11. Guo, Y.; Wei, X.; Gao, S.; Yue, W.; Li, Y.; Shen, G. Recent advances in carbon material-based multifunctional sensors and their applications in electronic skin systems. *Adv. Funct. Mater.* **2021**, *31*, 2104288. [CrossRef]
12. Cao, X.; Xiong, Y.; Sun, J.; Zhu, X.; Sun, Q.; Wang, Z.L. Piezoelectric nanogenerators derived self-powered sensors for multifunctional applications and artificial intelligence. *Adv. Funct. Mater.* **2021**, *31*, 2102983. [CrossRef]
13. Varghese, S.S.; Lonkar, S.; Singh, K.K.; Swaminathan, S.; Abdala, A. Recent advances in graphene based gas sensors. *Sens. Actuators B Chem.* **2015**, *218*, 160–183. [CrossRef]

14. Chakraborthy, A.; Nuthalapati, S.; Nag, A.; Afsarimanesh, N.; Alahi, M.E.E.; Altinsoy, M.E. A critical review of the use of graphene-based gas sensors. *Chemosensors* **2022**, *10*, 355. [CrossRef]

15. Pei, Y.; Zhang, X.; Hui, Z.; Zhou, J.; Huang, X.; Sun, G.; Huang, W. $Ti_3C_2T_X$ MXene for sensing applications: Recent progress, design principles, and future perspectives. *ACS Nano* **2021**, *15*, 3996–4017. [CrossRef]

16. Lee, E.; Yoon, Y.S.; Kim, D.-J. Two-dimensional transition metal dichalcogenides and metal oxide hybrids for gas sensing. *ACS Sens.* **2018**, *3*, 2045–2060. [CrossRef] [PubMed]

17. Abbas, A.N.; Liu, B.; Chen, L.; Ma, Y.; Cong, S.; Aroonyadet, N.; Köpf, M.; Nilges, T.; Zhou, C. Black phosphorus gas sensors. *ACS Nano* **2015**, *9*, 5618–5624. [CrossRef] [PubMed]

18. Bhargava Reddy, M.S.; Kailasa, S.; Marupalli, B.C.; Sadasivuni, K.K.; Aich, S. A family of 2D-MXenes: Synthesis, properties, and gas sensing applications. *ACS Sens.* **2022**, *7*, 2132–2163. [CrossRef] [PubMed]

19. Liu, M.; Chen, Y.-J.; Huang, X.; Dong, L.-Z.; Lu, M.; Guo, C.; Yuan, D.; Chen, Y.; Xu, G.; Li, S.-L.; et al. Porphyrin-Based COF 2D Materials: Variable Modification of Sensing Performances by Post-Metallization. *Angew. Chem. Int. Ed.* **2022**, *61*, e202115308. [CrossRef]

20. Wang, C.; Xia, K.; Wang, H.; Liang, X.; Yin, Z.; Zhang, Y. Advanced carbon for flexible and wearable electronics. *Adv. Mater.* **2019**, *31*, 1801072. [CrossRef]

21. Nag, A.; Mitra, A.; Mukhopadhyay, S.C. Graphene and its sensor-based applications: A review. *Sens. Actuators A Phys.* **2018**, *270*, 177–194. [CrossRef]

22. Chen, Z.; Wang, J.; Wang, Y. Strategies for the performance enhancement of graphene-based gas sensors: A review. *Talanta* **2021**, *235*, 122745. [CrossRef] [PubMed]

23. Katsnelson, M.I.; Novoselov, K.S.; Geim, A.K. Chiral tunnelling and the Klein paradox in graphene. *Nat. Phys.* **2006**, *2*, 620–625. [CrossRef]

24. Meng, Z.; Stolz, R.M.; Mendecki, L.; Mirica, K.A. Electrically-transduced chemical sensors based on two-dimensional nanomaterials. *Chem. Rev.* **2019**, *119*, 478–598. [CrossRef] [PubMed]

25. Reddeppa, M.; Mitta, S.B.; Chandrakalavathi, T.; Park, B.-G.; Murali, G.; Jeyalakshmi, R.; Kim, S.-G.; Park, S.H.; Kim, M.-D. Solution-processed Au@ rGO/GaN nanorods hybrid-structure for self-powered UV, visible photodetector and CO gas sensors. *Curr. Appl. Phys.* **2019**, *19*, 938–945. [CrossRef]

26. Cui, G.; Cheng, Y.; Liu, C.; Huang, K.; Li, J.; Wang, P.; Duan, X.; Chen, K.; Liu, K.; Liu, Z. Massive growth of graphene quartz fiber as a multifunctional electrode. *ACS Nano* **2020**, *14*, 5938–5945. [CrossRef]

27. Wu, J.; Wu, Z.; Ding, H.; Wei, Y.; Yang, X.; Li, Z.; Yang, B.-R.; Liu, C.; Qiu, L.; Wang, X. Multifunctional and high-sensitive sensor capable of detecting humidity, temperature, and flow stimuli using an integrated microheater. *ACS Appl. Mater. Interfaces* **2019**, *11*, 43383–43392. [CrossRef]

28. Lu, L.; Yang, B.; Liu, J. Flexible multifunctional graphite nanosheet/electrospun-polyamide 66 nanocomposite sensor for ECG, strain, temperature and gas measurements. *Chem. Eng. J.* **2020**, *400*, 125928. [CrossRef]

29. Yang, L.; Zheng, G.; Cao, Y.; Meng, C.; Li, Y.; Ji, H.; Chen, X.; Niu, G.; Yan, J.; Xue, Y.; et al. Moisture-resistant, stretchable NO_x gas sensors based on laser-induced graphene for environmental monitoring and breath analysis. *Microsyst. Nanoeng.* **2022**, *8*, 78. [CrossRef]

30. Mehta, S.S.; Nadargi, D.Y.; Tamboli, M.S.; Alshahrani, T.; Minnam Reddy, V.R.; Kim, E.S.; Mulla, I.S.; Park, C.; Suryavanshi, S.S. RGO/WO_3 hierarchical architectures for improved H_2S sensing and highly efficient solar-driving photo-degradation of RhB dye. *Sci. Rep.* **2021**, *11*, 5023. [CrossRef]

31. Li, S.; Zhang, Y.; Liang, X.; Wang, H.; Lu, H.; Zhu, M.; Wang, H.; Zhang, M.; Qiu, X.; Song, Y.; et al. Humidity-sensitive chemoelectric flexible sensors based on metal-air redox reaction for health management. *Nat. Commun.* **2022**, *13*, 5416. [CrossRef] [PubMed]

32. Zhang, C.; Ning, J.; Wang, B.; Guo, H.; Feng, X.; Shen, X.; Jia, Y.; Dong, J.; Wang, D.; Zhang, J.; et al. Hybridized 1T/2H-MoS_2/graphene fishnet tube for high-performance on-chip integrated micro-systems comprising supercapacitors and gas sensors. *Nano Res.* **2021**, *14*, 114–121. [CrossRef]

33. Shu, J.; Qiu, Z.; Tang, D. Self-referenced smartphone imaging for visual screening of H_2S using Cu_xO-polypyrrole conductive aerogel doped with graphene oxide framework. *Anal. Chem.* **2018**, *90*, 9691–9694. [CrossRef]

34. He, Q.; Wu, S.; Yin, Z.; Zhang, H. Graphene-based electronic sensors. *Chem. Sci.* **2012**, *3*, 1764–1772. [CrossRef]

35. Yuan, W.; Shi, G. Graphene-based gas sensors. *J. Mater. Chem. A* **2013**, *1*, 10078–10091. [CrossRef]

36. Yu, X.; Cheng, H.; Zhang, M.; Zhao, Y.; Qu, L.; Shi, G. Graphene-based smart materials. *Nat. Rev. Mater.* **2017**, *2*, 17046. [CrossRef]

37. Hu, H.; Yang, X.; Guo, X.; Khaliji, K.; Biswas, S.R.; García de Abajo, F.J.; Low, T.; Sun, Z.; Dai, Q. Gas identification with graphene plasmons. *Nat. Commun.* **2019**, *10*, 1131. [CrossRef]

38. Stanford, M.G.; Yang, K.; Chyan, Y.; Kittrell, C.; Tour, J.M. Laser-induced graphene for flexible and embeddable gas sensors. *ACS Nano* **2019**, *13*, 3474–3482. [CrossRef]

39. Kim, Y.J.; Kang, H.J.; Moerk, C.T.; Lee, B.-T.; Choi, J.S.; Yim, J.-H. Flexible, biocompatible, and electroconductive Polyurethane foam composites coated with graphene oxide for ammonia detection. *Sens. Actuators B Chem.* **2021**, *344*, 130269. [CrossRef]

40. Fang, H.; Lin, J.; Hu, Z.; Liu, H.; Tang, Z.; Shi, T.; Liao, G. $Cu(OH)_2$ nanowires/graphene oxide composites based QCM humidity sensor with fast-response for real-time respiration monitoring. *Sens. Actuators B Chem.* **2020**, *304*, 127313. [CrossRef]

41. Bi, S.; Hou, L.; Lu, Y. Multifunctional sodium alginate fabric based on reduced graphene oxide and polypyrrole for wearable closed-loop point-of-care application. *Chem. Eng. J.* **2021**, *406*, 126778. [CrossRef]

42. Zhang, L.; Tan, Q.; Wang, Y.; Fan, Z.; Lin, L.; Zhang, W.; Xiong, J. Wirelessly powered multi-functional wearable humidity sensor based on RGO-WS$_2$ heterojunctions. *Sens. Actuators B Chem.* **2021**, *329*, 129077. [CrossRef]

43. Xiong, C.; Li, M.; Zhao, W.; Duan, C.; Ni, Y. Flexible N-Doped reduced graphene oxide/carbon Nanotube-MnO$_2$ film as a multifunctional material for high-performance supercapacitors, catalysts and sensors. *J. Mater.* **2020**, *6*, 523–531. [CrossRef]

44. Chen, X.; Wang, T.; Han, Y.; Lv, W.; Li, B.; Su, C.; Zeng, M.; Yang, J.; Hu, N.; Su, Y.; et al. Wearable NO$_2$ sensing and wireless application based on ZnS nanoparticles/nitrogen-doped reduced graphene oxide. *Sens. Actuators B Chem.* **2021**, *345*, 130423. [CrossRef]

45. Allen, M.J.; Tung, V.C.; Kaner, R.B. Honeycomb carbon: A review of graphene. *Chem. Rev.* **2010**, *110*, 132–145. [CrossRef]

46. Majhi, S.M.; Mirzaei, A.; Kim, H.W.; Kim, S.S. Reduced graphene oxide (rGO)-loaded metal-oxide nanofiber gas sensors: An overview. *Sensors* **2021**, *21*, 1352. [CrossRef]

47. Achary, L.S.K.; Kumar, A.; Barik, B.; Nayak, P.S.; Tripathy, N.; Kar, J.P.; Dash, P. Reduced graphene oxide-CuFe$_2$O$_4$ nanocomposite: A highly sensitive room temperature NH$_3$ gas sensor. *Sens. Actuators B Chem.* **2018**, *272*, 100–109. [CrossRef]

48. Ogbeide, O.; Bae, G.; Yu, W.; Morrin, E.; Song, Y.; Song, W.; Li, Y.; Su, B.-L.; An, K.-S.; Hasan, T. Inkjet-printed rGO/binary metal oxide sensor for predictive gas sensing in a mixed environment. *Adv. Funct. Mater.* **2022**, *32*, 2113348. [CrossRef]

49. Chen, Z.; Guo, H.; Zhang, F.; Li, X.; Yu, J.; Chen, X. Porous ZnO/rGO nanosheet-based NO$_2$ gas sensor with high sensitivity and ppb-level detection limit at room temperature. *Adv. Mater. Interfaces* **2021**, *8*, 2101511. [CrossRef]

50. Bie, C.; Yu, H.; Cheng, B.; Ho, W.; Fan, J.; Yu, J. Design, fabrication, and mechanism of nitrogen-doped graphene-based photocatalyst. *Adv. Mater.* **2021**, *33*, 2003521. [CrossRef]

51. Mirzaei, A.; Bharath, S.P.; Kim, J.-Y.; Pawar, K.K.; Kim, H.W.; Kim, S.S. N-Doped Graphene and its derivatives as resistive gas sensors: An overview. *Chemosensors* **2023**, *11*, 334. [CrossRef]

52. Ali, M.; Afzal, A.M.; Iqbal, M.W.; Mumtaz, S.; Imran, M.; Ashraf, F.; Ur Rehman, A.; Muhammad, F. 2D-TMDs based electrode material for supercapacitor applications. *Int. J. Energy Res.* **2022**, *46*, 22336–22364. [CrossRef]

53. Zheng, W.; Liu, X.; Xie, J.; Lu, G.; Zhang, J. Emerging van der Waals junctions based on TMDs materials for advanced gas sensors. *Coord. Chem. Rev.* **2021**, *447*, 214151. [CrossRef]

54. Kuc, A.; Zibouche, N.; Heine, T. Influence of quantum confinement on the electronic structure of the transition metal sulfide *TS*$_2$. *Phys. Rev. B* **2011**, *83*, 245213. [CrossRef]

55. Yin, X.; Tang, C.S.; Zheng, Y.; Gao, J.; Wu, J.; Zhang, H.; Chhowalla, M.; Chen, W.; Wee, A.T.S. Recent developments in 2D transition metal dichalcogenides: Phase transition and applications of the (quasi-) metallic phases. *Chem. Soc. Rev.* **2021**, *50*, 10087–10115. [CrossRef]

56. Chhowalla, M.; Liu, Z.; Zhang, H. Two-dimensional transition metal dichalcogenide (TMD) nanosheets. *Chem. Soc. Rev.* **2015**, *44*, 2584–2586. [CrossRef]

57. Zhang, X.; Lai, Z.; Ma, Q.; Zhang, H. Novel structured transition metal dichalcogenide nanosheets. *Chem. Soc. Rev.* **2018**, *47*, 3301–3338. [CrossRef]

58. Qiao, X.-Q.; Zhang, Z.-W.; Hou, D.-F.; Li, D.-S.; Liu, Y.; Lan, Y.-Q.; Zhang, J.; Feng, P.; Bu, X. Tunable MoS$_2$/SnO$_2$ P–N heterojunctions for an efficient trimethylamine gas sensor and 4-nitrophenol reduction catalyst. *ACS Sustain. Chem. Eng.* **2018**, *6*, 12375–12384. [CrossRef]

59. Qin, Z.; Song, X.; Wang, J.; Li, X.; Wu, C.; Wang, X.; Yin, X.; Zeng, D. Development of flexible paper substrate sensor based on 2D WS$_2$ with S defects for room-temperature NH$_3$ gas sensing. *Appl. Surf. Sci.* **2022**, *573*, 151535. [CrossRef]

60. Islam, M.A.; Li, H.; Moon, S.; Han, S.S.; Chung, H.-S.; Ma, J.; Yoo, C.; Ko, T.-J.; Oh, K.H.; Jung, Y.; et al. Vertically aligned 2D MoS$_2$ layers with strain-engineered serpentine patterns for high-performance stretchable gas sensors: Experimental and theoretical demonstration. *ACS Appl. Mater. Interfaces* **2020**, *12*, 53174–53183. [CrossRef]

61. Afzal, A.M.; Iqbal, M.Z.; Dastgeer, G.; Nazir, G.; Mumtaz, S.; Usman, M.; Eom, J. WS$_2$/GeSe/WS$_2$ bipolar transistor-based chemical sensor with fast response and recovery times. *ACS Appl. Mater. Interfaces* **2020**, *12*, 39524–39532. [CrossRef] [PubMed]

62. Dong, X.; Chen, T.; Liu, G.; Xie, L.; Zhou, G.; Long, M. Multifunctional 2D g-C$_4$N$_3$/MoS$_2$ vdW heterostructure-based nanodevices: Spin filtering and gas sensing properties. *ACS Sens.* **2022**, *7*, 3450–3460. [CrossRef] [PubMed]

63. Yang, C.; Xie, J.; Lou, C.; Zheng, W.; Liu, X.; Zhang, J. Flexible NO$_2$ sensors based on WSe$_2$ nanosheets with bifunctional selectivity and superior sensitivity under UV activation. *Sens. Actuators B Chem.* **2021**, *333*, 129571. [CrossRef]

64. Huang, Y.; Jiao, W.; Chu, Z.; Nie, X.; Wang, R.; He, X. SnS$_2$ quantum dot-based optoelectronic flexible sensors for ultrasensitive detection of NO$_2$ down to 1 ppb. *ACS Appl. Mater. Interfaces* **2020**, *12*, 25178–25188. [CrossRef] [PubMed]

65. Peng, Z.; Tao, L.-Q.; Zou, S.; Zhu, C.; Wang, G.; Sun, H.; Ren, T.-L. A multi-functional NO$_2$ gas monitor and self-alarm based on laser-induced graphene. *Chem. Eng. J.* **2022**, *428*, 131079. [CrossRef]

66. Wang, B.; Luo, H.; Wang, X.; Wang, E.; Sun, Y.; Tsai, Y.-C.; Dong, J.; Liu, P.; Li, H.; Xu, Y. et, al. Direct laser patterning of two-dimensional lateral transition metal disulfide-oxide-disulfide heterostructures for ultrasensitive sensors. *Nano Res.* **2020**, *13*, 2035–2043. [CrossRef]

67. Wang, Z.; Jing, X.; Duan, S.; Liu, C.; Kang, D.; Xu, X.; Chen, J.; Xia, Y.; Chang, B.; Zhao, C.; et al. 2D PtSe$_2$ enabled wireless wearable gas monitoring circuits with distinctive strain-enhanced performance. *ACS Nano* **2023**, *17*, 11557–11566. [CrossRef]

68. Liu, Z.; Wang, H.; Cao, H.; Xie, D.; Li, C.; Yang, H.; Yao, W.; Cheetham, A.K. Ultratough hydrogen-bond-bridged phosphorene films. *Adv. Mater.* **2022**, *34*, 2203332. [CrossRef]

69. VahidMohammadi, A.; Rosen, J.; Gogotsi, Y. The world of two-dimensional carbides and nitrides (MXenes). *Science* **2021**, *372*, eabf1581. [CrossRef]

70. Chen, H.; Ma, H.; Zhang, P.; Wen, Y.; Qu, L.; Li, C. Pristine titanium carbide MXene hydrogel matrix. *ACS Nano* **2020**, *14*, 10471–10479. [CrossRef]

71. Anasori, B.; Xie, Y.; Beidaghi, M.; Lu, J.; Hosler, B.C.; Hultman, L.; Kent, P.R.; Gogotsi, Y.; Barsoum, M.W. Two-dimensional, ordered, double transition metals carbides (MXenes). *ACS Nano* **2015**, *9*, 9507–9516. [CrossRef] [PubMed]

72. Wang, D.; Zhang, D.; Guo, J.; Hu, Y.; Yang, Y.; Sun, T.; Zhang, H.; Liu, X. Multifunctional poly (vinyl alcohol)/Ag nanofibers-based triboelectric nanogenerator for self-powered MXene/tungsten oxide nanohybrid NO_2 gas sensor. *Nano Energy* **2021**, *89*, 106410. [CrossRef]

73. Zhou, T.; Zhang, P.; Yu, Z.; Tao, M.; Zhou, D.; Yang, B.; Zhang, T. Light-driven, ultra-sensitive and multifunctional ammonia wireless sensing system by plasmonic-functionalized Nb_2CT_x MXenes towards smart agriculture. *Nano Energy* **2023**, *108*, 108216. [CrossRef]

74. Wang, D.; Zhang, D.; Yang, Y.; Mi, Q.; Zhang, J.; Yu, L. Multifunctional latex/polytetrafluoroethylene-based triboelectric nanogenerator for self-powered organ-like MXene/metal–organic framework-derived CuO nanohybrid ammonia sensor. *ACS Nano* **2021**, *15*, 2911–2919. [CrossRef]

75. Wang, D.; Zhang, D.; Chen, X.; Zhang, H.; Tang, M.; Wang, J. Multifunctional respiration-driven triboelectric nanogenerator for self-powered detection of formaldehyde in exhaled gas and respiratory behavior. *Nano Energy* **2022**, *102*, 107711. [CrossRef]

76. Wang, X.; Gong, L.; Li, Z.; Yin, Y.; Zhang, D. A room temperature ammonia gas sensor based on cerium oxide/MXene and self-powered by a freestanding-mode triboelectric nanogenerator and its multifunctional monitoring application. *J. Mater. Chem. A* **2023**, *11*, 7690–7701. [CrossRef]

77. Sardana, S.; Kaur, H.; Arora, B.; Aswal, D.K.; Mahajan, A. Self-powered monitoring of ammonia using an $MXene/TiO_2$/cellulose nanofiber heterojunction-based sensor driven by an electrospun triboelectric nanogenerator. *ACS Sens.* **2022**, *7*, 312–321. [CrossRef]

78. Liu, L.-X.; Chen, W.; Zhang, H.-B.; Wang, Q.-W.; Guan, F.; Yu, Z.-Z. Flexible and multifunctional silk textiles with biomimetic leaf-like MXene/silver nanowire nanostructures for electromagnetic interference shielding, humidity monitoring, and self-derived hydrophobicity. *Adv. Funct. Mater.* **2019**, *29*, 1905197. [CrossRef]

79. He, S.; Gui, Y.; Wang, Y.; Yang, J. A self-powered β-Ni(OH)$_2$/MXene based ethanol sensor driven by an enhanced triboelectric nanogenerator based on β-Ni(OH)$_2$@PVDF at room temperature. *Nano Energy* **2023**, *107*, 108132. [CrossRef]

80. Jin, X.; Li, L.; Zhao, S.; Li, X.; Jiang, K.; Wang, L.; Shen, G. Assessment of occlusal force and local gas release using degradable bacterial cellulose/$Ti_3C_2T_x$ MXene bioaerogel for oral healthcare. *ACS Nano* **2021**, *15*, 18385–18393. [CrossRef]

81. Zhao, X.; Wang, L.-Y.; Tang, C.-Y.; Zha, X.-J.; Liu, Y.; Su, B.-H.; Ke, K.; Bao, R.-Y.; Yang, M.-B.; Yang, W. Smart $Ti_3C_2T_x$ MXene fabric with fast humidity response and joule heating for healthcare and medical therapy applications. *ACS Nano* **2020**, *14*, 8793–8805. [CrossRef] [PubMed]

82. Fan, F.-R.; Tian, Z.-Q.; Wang, Z.L. Flexible triboelectric generator. *Nano Energy* **2012**, *1*, 328–334. [CrossRef]

83. Ding, X.; Zhang, Y.; Zhang, Y.; Ding, X.; Zhang, H.; Cao, T.; Qu, Z.-B.; Ren, J.; Li, L.; Guo, Z. Modular assembly of MXene frameworks for noninvasive disease diagnosis via urinary volatiles. *ACS Nano* **2022**, *16*, 17376–17388. [CrossRef]

84. Wang, R.; Yan, X.; Ge, B.; Zhou, J.; Wang, M.; Zhang, L.; Jiao, T. Facile preparation of self-assembled black phosphorus-dye composite films for chemical gas sensors and surface-enhanced Raman scattering performances. *ACS Sustain. Chem. Eng.* **2020**, *8*, 4521–4536. [CrossRef]

85. Smith, M.K.; Jensen, K.E.; Pivak, P.A.; Mirica, K.A. Direct self-assembly of conductive nanorods of metal–organic frameworks into chemiresistive devices on shrinkable polymer films. *Chem. Mater.* **2016**, *28*, 5264–5268. [CrossRef]

86. Smith, M.K.; Mirica, K.A. Self-organized frameworks on textiles (SOFT): Conductive fabrics for simultaneous sensing, capture, and filtration of gases. *J. Am. Chem. Soc.* **2017**, *139*, 16759–16767. [CrossRef]

87. Reddeppa, M.; KimPhung, N.T.; Murali, G.; Pasupuleti, K.S.; Park, B.-G.; In, I.; Kim, M.-D. Interaction activated interfacial charge transfer in 2D g-C_3N_4/GaN nanorods heterostructure for self-powered UV photodetector and room temperature NO_2 gas sensor at ppb level. *Sens. Actuators B Chem.* **2021**, *329*, 129175. [CrossRef]

88. Khasim, S.; Pasha, A.; Dastager, S.G.; Panneerselvam, C.; Hamdalla, T.A.; Al-Ghamdi, S.A.; Alfadhli, S.; Makandar, M.B.; Albalawi, J.B.; Darwish, A.A.A. Design and development of multi-functional graphitic carbon nitride heterostructures embedded with copper and iron oxide nanoparticles as versatile sensing platforms for environmental and agricultural applications. *Ceram. Int.* **2023**, *49*, 20688–20698. [CrossRef]

89. Malik, R.; Tomer, V.K.; Joshi, N.; Dankwort, T.; Lin, L.; Kienle, L. Au–TiO_2-loaded cubic g-C_3N_4 nanohybrids for photocatalytic and volatile organic amine sensing applications. *ACS Appl. Mater. Interfaces* **2018**, *10*, 34087–34097. [CrossRef]

90. Sethuraman, S.; Marimuthu, A.; Kattamuthu, R.; Karuppasamy, G. Highly surface active niobium doped g-C_3N_4/g-C_3N_4 heterojunction interface towards superior photocatalytic and selective ammonia response. *Appl. Surf. Sci.* **2021**, *561*, 150077. [CrossRef]

91. Li, H.; Sun, Y.; Zhang, Q.; Yuan, H.; Dong, C.; Xu, S.; Xu, M. Facile synthesis of ZnO/Ag/g-C_3N_4 nanocomposites for multiple applications in photocatalytic degradation and photoactivated NO_2 sensing. *Appl. Surf. Sci.* **2023**, *638*, 158010. [CrossRef]

92. Gong, L.; Wang, X.; Zhang, D.; Ma, X.; Yu, S. Flexible wearable humidity sensor based on cerium oxide/graphitic carbon nitride nanocomposite self-powered by motion-driven alternator and its application for human physiological detection. *J. Mater. Chem. A* **2021**, *9*, 5619–5629. [CrossRef]

93. Ko, M.; Mendecki, L.; Mirica, K.A. Conductive two-dimensional metal–organic frameworks as multifunctional materials. *Chem. Commun.* **2018**, *54*, 7873–7891. [CrossRef]

94. Dong, M.-M.; He, H.; Wang, C.-K.; Fu, X.-X. Two-dimensional MoSi$_2$As$_4$-based field-effect transistors integrating switching and gas-sensing functions. *Nanoscale* **2023**, *15*, 9106–9115. [CrossRef] [PubMed]

95. Zhang, L.; Li, Z.; Yang, J.; Zhou, J.; Zhang, Y.; Zhang, H.; Li, Y. A fully integrated flexible tunable chemical sensor based on gold-modified indium selenide nanosheets. *ACS Sens.* **2022**, *7*, 1183–1193. [CrossRef] [PubMed]

96. Yang, S.; Jiang, C.; Wei, S.-H. Gas sensing in 2D materials. *Appl. Phys. Rev.* **2017**, *4*, 021304. [CrossRef]

97. Sharma, A.; Rout, C.S. Advances in understanding the gas sensing mechanisms by *in situ* and *operando* spectroscopy. *J. Mater. Chem. A* **2021**, *9*, 18175–18207. [CrossRef]

98. Kim, S.; Kwak, D.H.; Choi, I.; Hwang, J.; Kwon, B.; Lee, E.; Ye, J.; Lim, H.; Cho, K.; Chung, H.-J.; et al. Enhanced gas sensing properties of graphene transistor by reduced doping with hydrophobic polymer brush as a surface modification layer. *ACS Appl. Mater. Interfaces* **2020**, *12*, 55493–55500. [CrossRef]

99. Wu, J.; Feng, S.; Li, Z.; Tao, K.; Chu, J.; Miao, J.; Norford, L.K. Boosted sensitivity of graphene gas sensor via nanoporous thin film structures. *Sens. Actuators B Chem.* **2018**, *255*, 1805–1813. [CrossRef]

100. Zhang, D.; Wu, Z.; Zong, X. Flexible and highly sensitive H$_2$S gas sensor based on in-situ polymerized SnO2/rGO/PANI ternary nanocomposite with application in halitosis diagnosis. *Sens. Actuators B Chem.* **2019**, *289*, 32–41. [CrossRef]

101. Wu, T.-Y.; Chen, Y.-Z.; Wang, Y.-C.; Tang, S.-Y.; Shih, Y.-C.; Cheng, F.; Wang, Z.M.; Lin, H.-N.; Chueh, Y.-L. Highly sensitive, selective and stable NO$_2$ gas sensors with a ppb-level detection limit on 2D-platinum diselenide films. *J. Mater. Chem. C* **2020**, *8*, 4851–4858.

102. Long, H.; Harley-Trochimczyk, A.; Pham, T.; Tang, Z.; Shi, T.; Zettl, A.; Carraro, C.; Worsley, M.A.; Maboudian, R. High surface area MoS$_2$/Graphene hybrid aerogel for ultrasensitive NO$_2$ detection. *Adv. Funct. Mater.* **2016**, *26*, 5158–5165. [CrossRef]

103. Chen, W.Y.; Jiang, X.; Lai, S.-N.; Peroulis, D.; Stanciu, L. Nanohybrids of a MXene and transition metal dichalcogenide for selective detection of volatile organic compounds. *Nat. Commun.* **2020**, *11*, 1302. [CrossRef] [PubMed]

104. Lee, E.; VahidMohammadi, A.; Yoon, Y.S.; Beidaghi, M.; Kim, D.-J. Two-dimensional vanadium carbide MXene for gas sensors with ultrahigh sensitivity toward nonpolar gases. *ACS Sens.* **2019**, *4*, 1603–1611. [CrossRef]

105. Zhang, L.; Li, Z.; Liu, J.; Peng, Z.; Zhou, J.; Zhang, H.; Li, Y. Optoelectronic gas sensor based on few-layered InSe nanosheets for NO$_2$ detection with ultrahigh antihumidity ability. *Anal. Chem.* **2020**, *92*, 11277–11287. [CrossRef]

106. Liu, Z.; Huang, J.; Wang, Q.; Zhou, J.; Ye, J.; Li, X.; Geng, Y.; Liang, Z.; Du, Y.; Tian, X. Indium oxide-black phosphorus composites for ultrasensitive nitrogen dioxide sensing at room temperature. *Sens. Actuators B Chem.* **2020**, *308*, 127650. [CrossRef]

107. Akhtar, A.; Jiao, C.; Chu, X.; Liang, S.; Dong, Y.; He, L. Acetone sensing properties of the g–C$_3$N$_4$–CuO nanocomposites prepared by hydrothermal method. *Mater. Chem. Phys.* **2021**, *265*, 124375. [CrossRef]

108. Chen, Z.; Chen, Z.; Song, Z.; Ye, W.; Fan, Z. Smart gas sensor arrays powered by artificial intelligence. *J. Semicond.* **2019**, *40*, 111601. [CrossRef]

109. Viejo, C.G.; Fuentes, S.; Godbole, A.; Widdicombe, B.; Unnithan, R.R. Development of a low-cost e-nose to assess aroma profiles: An artificial intelligence application to assess beer quality. *Sens. Actuators B Chem.* **2020**, *308*, 127688. [CrossRef]

110. Choi, K.H.; Oh, S.; Chae, S.; Jeong, B.J.; Kim, B.J.; Jeon, J.; Lee, S.H.; Yoon, S.O.; Woo, C.; Dong, X.; et al. Transition metal thiophosphates Nb$_4$P$_2$S$_{21}$: New kind of 2D materials for multi-functional sensors. *J. Alloys Compd.* **2021**, *864*, 158811. [CrossRef]

111. Liu, G.; Chen, T.; Li, X.; Xu, Z.; Xiao, X. Electronic transport in biphenylene network monolayer: Proposals for 2D multifunctional carbon-based nanodevices. *Appl. Surf. Sci.* **2022**, *599*, 153993. [CrossRef]

112. Wan, X.; Yu, W.; Wang, A.; Wang, X.; Robertson, J.; Zhang, Z.; Guo, Y. High-throughput screening of gas sensor materials for decomposition products of eco-friendly insulation medium by machine learning. *ACS Sens.* **2023**, *8*, 2319–2330. [CrossRef] [PubMed]

113. Mohammadzadeh, M.R.; Hasani, A.; Jaferzadeh, K.; Fawzy, M.; Silva, T.D.; Abnavi, A.; Ahmadi, R.; Ghanbari, H.; Askar, A.; Kabir, F.; et al. Unique photoactivated time-resolved response in 2D GeS for selective detection of volatile organic compounds. *Adv. Sci.* **2023**, *10*, 2205458. [CrossRef]

114. Huang, S.; Croy, A.; Panes-Ruiz, L.A.; Khavrus, V.; Bezugly, V.; Ibarlucea, B.; Cuniberti, G. Machine learning-enabled smart gas sensing platform for identification of industrial gases. *Adv. Intell. Syst.* **2022**, *4*, 2200016. [CrossRef]

115. Yaqoob, U.; Younis, M.I. Chemical gas sensors: Recent developments, challenges, and the potential of machine learning—A review. *Sensors* **2021**, *21*, 2877. [CrossRef]

116. Ye, Z.; Liu, Y.; Li, Q. Recent progress in smart electronic nose technologies enabled with machine learning methods. *Sensors* **2021**, *21*, 7620. [CrossRef]